

Run15 J/ψ Multiplicity Dependence Analysis

Yasser Corrales Morales¹, Cameron Dean¹, Zhaozhong Shi¹, Ajeeta Khatiwada¹, Cesar Da Silva¹, Sanghoon Lim², Haiwang Yu³, and Ming Liu¹

¹Los Alamos National Laboratory

²Pusan National University

³Brookhaven National Laboratory

Abstract

This analysis note summarizes the technical details of the run15pp event multiplicity-dependent relative J/ψ yield analysis. The event multiplicity is determined by the PHENIX silicon detectors, the FVTX and SVX, which cover the pseudorapidity ranges $1.2 < |\eta| < 2.4$ and $|\eta| < 1.0$, respectively. The J/ψ candidates are measured by the two muon arms in the rapidity range of $1.2 < |y| < 2.2$. Our results show the relative yield of J/ψ mesons per $p + p$ collision increases with the event multiplicity, indicating possible multi-parton interactions in $p + p$ collisions.

Contents

1	Analysis Organization	2
2	Introduction	4
3	Run15 QA and good run lists: p+p	6
3.1	Run15 p+p MB run QA	7
3.2	Run15 p+p MU run QA	11
4	Run15pp MB and Muon Data Analysis	13
4.1	MB Event and FVTX and SVX tracklet selection	14
4.2	Run15pp Event Multiplicity Studies	16
4.3	Multiple p+p collisions and event multiplicity	17
4.4	Run15pp MB Trigger bias analysis	22
4.5	p+p MU analysis: <i>J/ψ</i> <i>SignalExtraction</i>	25
4.6	Closure Test of Unbinned Fit	38
5	Systematic Error Analysis	45
5.1	Event multiplicity dependent <i>J/ψ</i> reconstruction efficiency	45
5.2	<i>J/ψ</i> fitting	45
5.3	MB Trigger Bias Systematic Uncertainties	49
5.4	Systematic Uncertainties on the Evaluation of Multiple Collisions	51
5.5	Systematic Uncertainties on <i>J/ψ</i> Reconstruction	51
5.6	Summary of Systematic Uncertainties	51
6	Results	53
6.1	\hat{Y} vs \hat{N}_{trk} Before Corrections	53
6.2	\hat{Y} vs \hat{N}_{trk} After Corrections	53

1 Analysis Organization

The idea of studying event multiplicity dependence of J/ψ production in small systems in PHENIX went back to early 2013 when several collaborators investigated the relative yields of J/ψ as a function of event multiplicity determined by the FVTX detector in $p + p$ collisions at $\sqrt{s} = 510$ GeV. [3]

Here is the analysis flow chart of major steps with code locations in RCF (working directories):

Run15pp(pAu) J/Psi Multiplicity Analysis Flow Chart

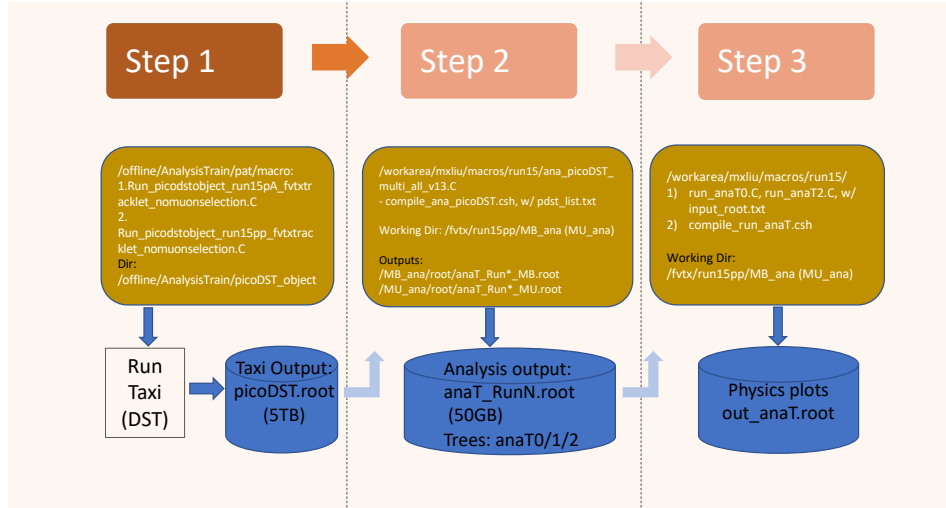


Figure 1: Analysis flow chart with major code, input and output file locations.

In this analysis, we have used 3 data sets; MB, MU and OT, from run15pp production (pro108):

Run15pp MB pDST taxi output files:

`/gpfs/mnt/gpfs02/phenix/spin/spin1/phnxsp01/mxliu/taxi/Run15pp200CAMP108/17698/data`

Run15pp MU pDST taxi output files:

`/gpfs/mnt/gpfs02/phenix/spin/spin1/phnxsp01/mxliu/taxi/Run15pp200CAMUP108/17697/data`

Run15pp OT pDST taxi output files:

`/gpfs/mnt/gpfs02/phenix/hhj/hhj1/mxliu/taxi/Run15pp200CA0TP108/17975/data`

All macros can be found on PHENIX CVS repository:

`/afs/rhic/phenix/PHENIX_CVS/offline/analysis/run15-jpsi_multiplicity_ana`

`(/direct/phenix+u/workarea/mxliu/offline/analysis/run15-jpsi_multiplicity_ana)`

To obtain the final results, shown as *Step 3* in Fig. 1, several different macros were used to ensure the steps were taken in the appropriate order. The latest work-in-progress analysis macros are saved on github: <https://github.com/MYOMAO/PHENIXJPsiAna>

They are also copied to the above CVS directory.

The folders of macros are organized as follows:

- SKIM: the skimming of the data files before the analysis
- SIGNALEXTRACTION: the unbinned fit macros for J/ψ signal extraction
- MBSTAT: the estimation of number of MB events with the application of prescale factors
- TRIGBIAS: calculation the MB trigger efficiency bias as a function of multiplicity.
- FinalResults: put together the J/ψ signal raw yield, number of MB events, and the trigger bias to obtain the file \hat{R} results.

2 Introduction

This analysis note documents the measurements of the relative yield of J/ψ mesons as a function of event multiplicity determined by the FVTX and SVX detectors in $p + p$ collisions from PHENIX 2015 run.

Back in 2014, the relative J/ψ yield as a function of event multiplicity determined by the FVTX in 510 GeV $p + p$ collisions was studied using data collected by the PHENIX experiment in 2013 [3]. The analysis did not reach completion due to early departure of one of our collaborators from the PHENIX experiment, and our focus was shifted to other physics measurements. The primary physics goal is to investigate J/ψ production mechanisms in high energy hadronic interactions in $p + p$ collisions, including both initial state and final state effects. In 2015, the PHENIX experiment took highest luminosity data of $p + p$, $p + Au$ and $p + Al$ collisions at a center of mass energy of $\sqrt{s} = 200$ GeV. This provides a unique opportunity for us to further explore various contributions to the J/ψ production in hadronic interactions.

Fig. 2 shows various different event topologies that can appear during the decay of a J/ψ meson that can also be measured by the PHENIX forward muon spectrometers. The events multiplicity is determined by the FVTX and SVX silicon detectors.



Figure 2: J/ψ yields vs event multiplicity determined at various rapidities. In PHENIX, the two forward FVTX detectors cover pseudorapidity range $1.2 < |\eta| < 2.4$, and the central arm SVX covers $|\eta| < 1.0$.

We measure the relative yield of J/ψ as a function of the event multiplicity N_{trk} determined by FVTX and/or SVX silicon detectors per MB collision event:

$$Y^{J/\psi}(N_{\text{trk}}) = \frac{d\sigma^{J/\psi}/dN_{\text{trk}}}{d\sigma^{MB}/dN_{\text{trk}}} \quad (1)$$

We further define the normalized J/ψ yield $\hat{Y}^{J/\psi}$ vs event multiplicity,

$$\hat{Y}^{J/\psi}(N_{\text{trk}}) = \frac{d\sigma^{J/\psi}/dN_{\text{trk}}/\langle\sigma^{J/\psi}\rangle}{d\sigma^{MB}/dN_{\text{trk}}/\langle\sigma^{MB}\rangle} \quad (2)$$

where $\langle N_{\text{trk}}^{\text{MB}} \rangle$ is the normalized MB event multiplicity.

Experimentally, we measure the above relative yield with the following expression,

$$\hat{Y}(N_{\text{trk}}) = \frac{[N^{J/\psi}(N_{\text{trk}})/\epsilon^{J/\psi}(N_{\text{trk}})]/[N^{J/\psi}/\epsilon^{J/\psi}]}{[N^{\text{MB}}(N_{\text{trk}})/\epsilon^{\text{MB}}(N_{\text{trk}})]/[N^{\text{MB}}/\epsilon^{\text{MB}}]} \quad (3)$$

where $N^{J/\psi}(N_{\text{trk}})$ and $N^{\text{MB}}(N_{\text{trk}})$ are the raw counts of J/ψ and MB events in a given event multiplicity bin N_{trk} , respectively, and $\epsilon^{J/\psi, \text{MB}}(N_{\text{trk}})$ and $\epsilon^{J/\psi, \text{MB}}$ are the event multiplicity dependent and averaged J/ψ (or MB) efficiencies, respectively.

The overall efficiency of J/ψ or MB events is given by the product of detector acceptance, trigger efficiency and offline reconstruction efficiency:

$$\epsilon^{J/\psi, \text{MB}} = A_{\text{accept}} \times \epsilon_{\text{trig}} \times \epsilon_{\text{reco}} \quad (4)$$

In our analysis, J/ψ events are measured by the PHENIX forward muon spectrometers in the pseudorapidity range $1.2 < |\eta| < 2.2$, and MB events are tagged with hits in both BBC detectors, both J/ψ and MB events are required to have valid collision z-vertex within ± 10 cm. Event multiplicity N_{trk} are measured by 3 silicon detectors: (1) South FVTX (FVTXS); (2) North FVTX (FVTXN) and (3) Central SVX (SVX).

3 Run15 QA and good run lists: p+p

Good runs of $p + p$ data are selected based on previous run15 $p + p$ and $p + \text{Au}$ dimuon analyses [1]. Sanghoon has provided the latest bad runs for run15pp dimuon analysis, based on the previous analysis (PPG224) from which we derived the good run list:

```
/phenix/hhj/hhj1/shlim/work/15.run15/10.runQA/03.yield_run/Run15pp200_badrn_for_hadron_20161231.ro
```

A few more bad runs are removed from the analysis based on event multiplicity, and the quality assurance tests of the FVTXS, FVTXN and SVX. The final good run list for south and north arm dimuon analysis are located here:

- /fvtx/mxliu/run15pp/Common_MB_Good_North_v3.txt
- /fvtx/mxliu/run15pp/Common_MB_Good_South_v3.txt
- /fvtx/mxliu/run15pp/Common_MU_Good_North_v3.txt
- /fvtx/mxliu/run15pp/Common_MU_Good_South_v3.txt

The macros which were used to select bad and good runs are: `-plot_QA_run15pp_MB.C` and `anaRun_SelectRun_v2.C`

3.1 Run15 p+p MB run QA

We use the same dimuon good runs list selected in the PPG224 run15pp J/ψ analysis. For MB triggered events, we further require there are at least 100k events for each run.

In this analysis, MB events are selected from the $\text{BBCLL1}_{\text{narrowvtx}}$ trigger, which had an online BBC z-vertex cut around ± 15 cm. This trigger provides the highest number of MB samples for this analysis. The other two MB triggers, $\text{BBCLL1}_{\text{novtx}}$ and $\text{BBCLL1}_{\text{tube}>0}$ are also used to cross check collisions vertex distributions etc.

In the final analysis, the MB and J/ψ events are selected within a narrow z-vertex to have uniform event multiplicity acceptance in both the FVTX and SVX detectors.

- $|\text{Evt_vtxZ}| < 10$ cm
- $|\text{Evt_bbcZ}| < 20$ cm
- $1.2 < |\eta_{\text{FVTX}}| < 2.4$ for FVTX tracklets
- $|\eta_{\text{SVX}}| < 1$ for SVX tracklets

Fig. 3 shows the BBC rate ($\text{BBCLL1}_{\text{novtx}}$) distribution measured at the beginning of a run during the data taking. Typically, the BBC rate dropped by about 50 % from its peak value by the end of a fill (a fill is typically about 6 hours long), and within a run, the BBC rate typically dropped by 10% by the end of a run (typically corresponding to one hour of DAQ time). Fig. 4 shows the BBC rate vs run number distribution from run15pp MB events.

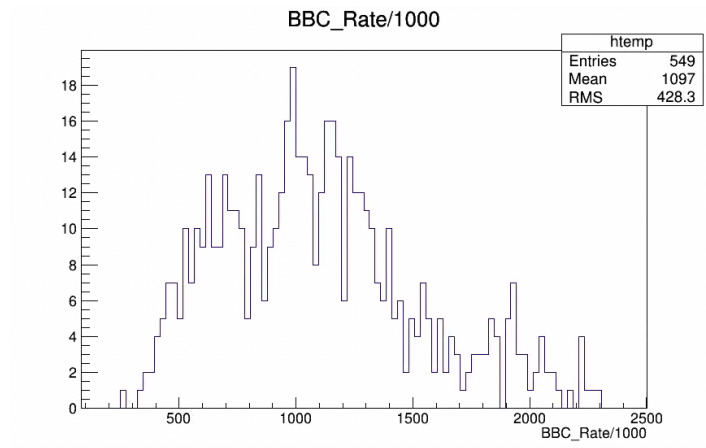


Figure 3: BBC rate [kHz] distribution of run15pp MB. The mean BBC rate is about 1,100 kHz.

For the analysis, the relevant rate is the luminosity weighted BBC rate. Fig. 5 shows the run luminosity weighted (by the total live $\text{BBCLL1}_{\text{narrowvtx}}$ trigger counts) BBC rate distribution. The mean luminosity-weighted BBC rate is about 830 kHz.

It was also checked that the run time and BBC rate dependence of the run-averaged event multiplicity $\langle \text{FVTXS} \rangle$, $\langle \text{FVTXN} \rangle$ and $\langle \text{SVX} \rangle$. Fig. 6 shows the averaged event multiplicity from FVTX, SVX and BBC as a function of RunNumber. It should be noted that the bad runs with mean values deviated from the central values by 3σ are rejected in the run QA process.

Fig. 7 shows the averaged event multiplicity from FVTX, SVX and BBC vs RunNumber. Runs with average multiplicity beyond $\pm 20\%$ of the mean value are removed.

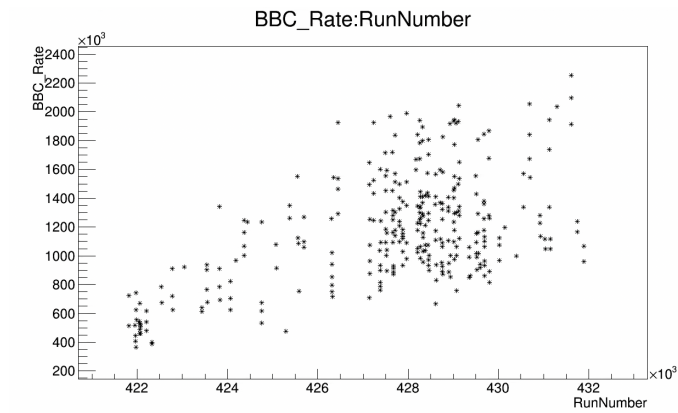


Figure 4: BBC rate [Hz] vs RunNumber of MB from run15pp.

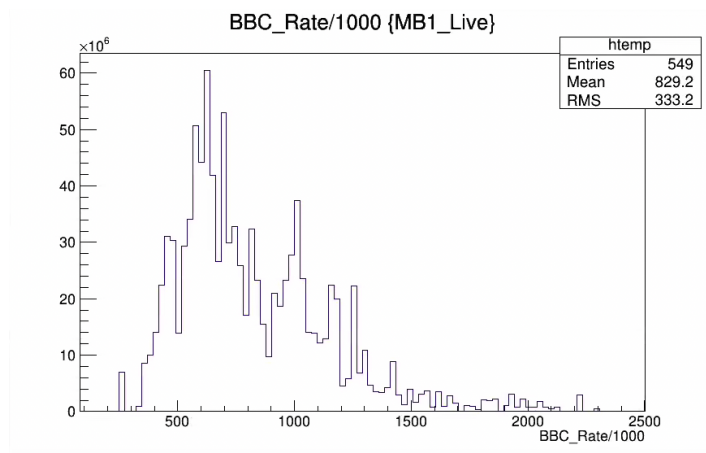


Figure 5: Run luminosity (BBCLL1_narrowvtx) weighted BBC rate distributions of MB runs. The mean BBC rate is about 830kHz

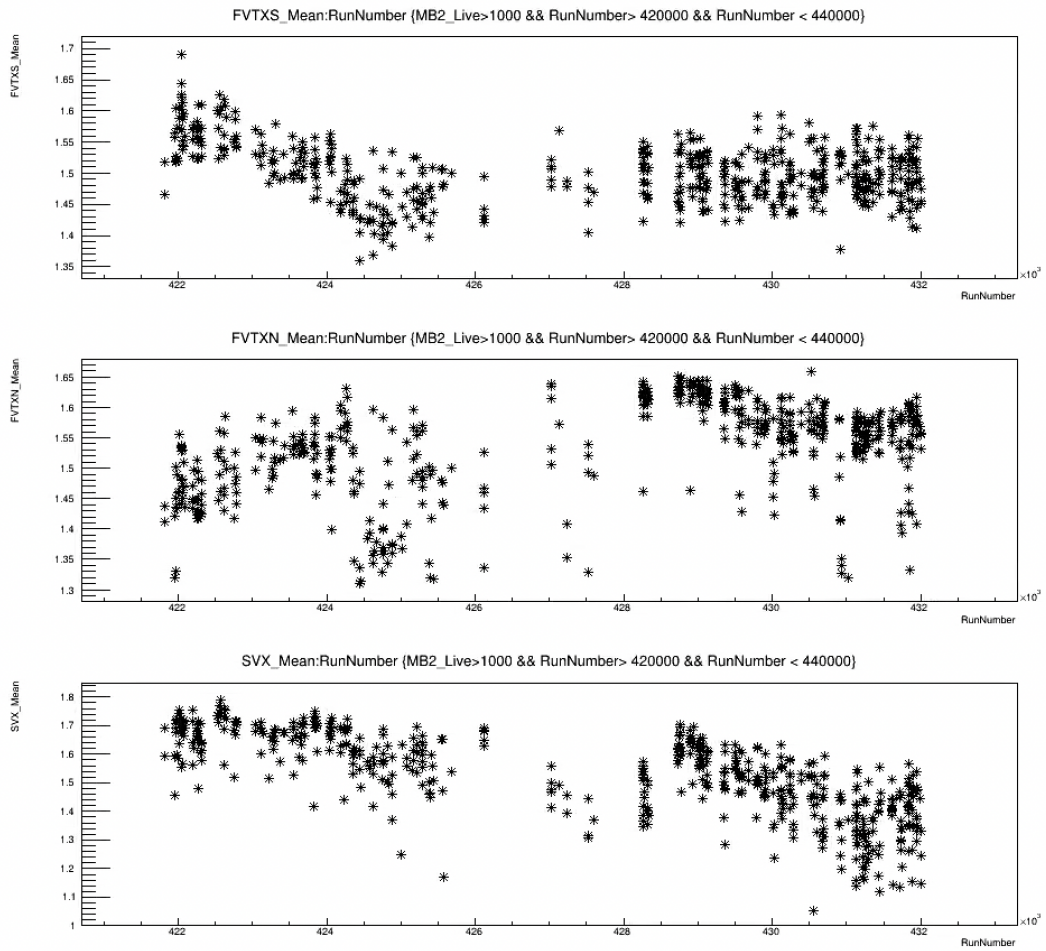


Figure 6: MB events' run averaged Evt.Mult. (FVTXS, FVTXN and SVX) vs RunNumber.

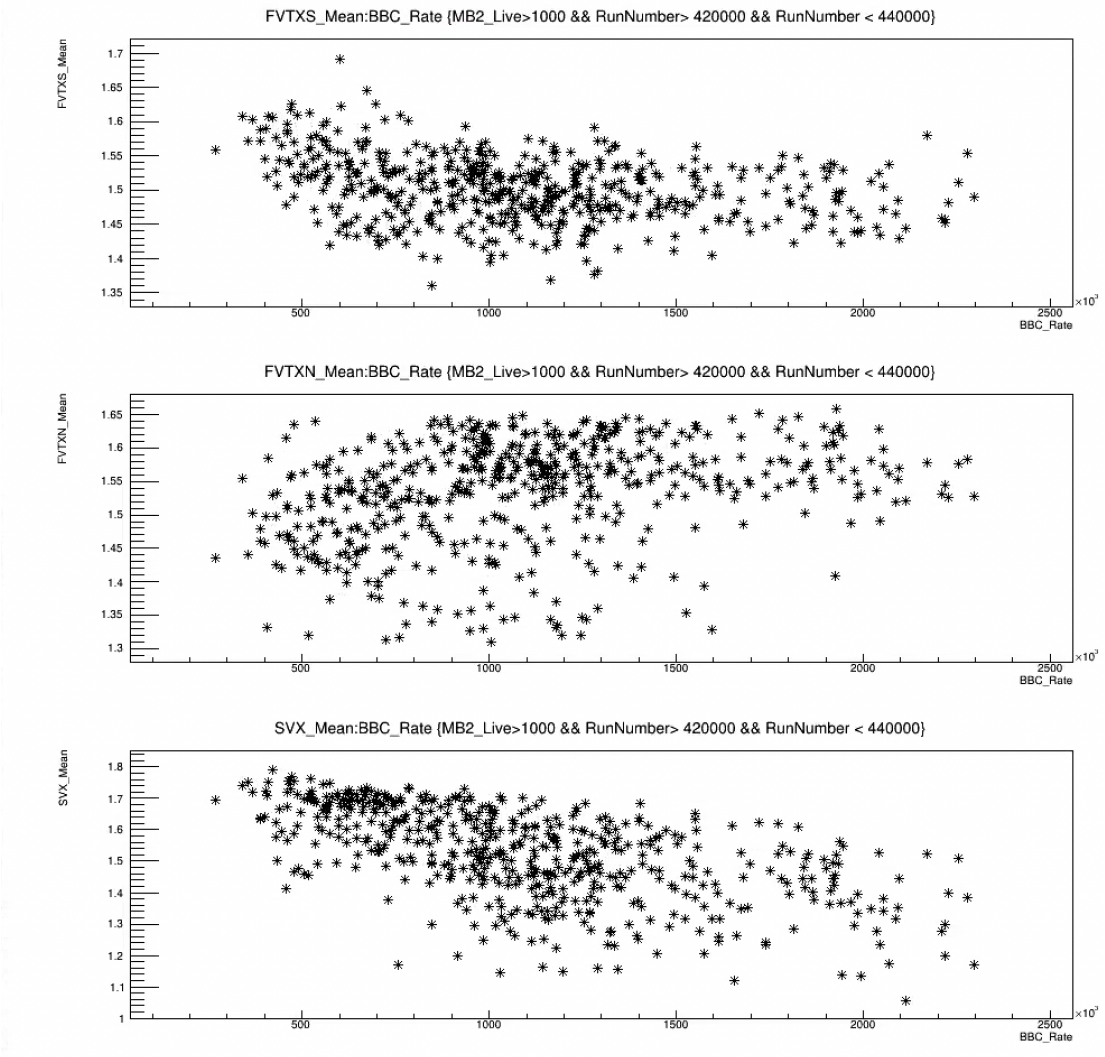


Figure 7: MB events' run averaged Evt_Mult_(FVTXS, FVTXN and SVX) vs BBC rate measured at the beginning of a run.

3.2 Run15 p+p MU run QA

To select dimuon events, we apply the following cuts:

- $|\text{Evt_vtxZ}| < 10\text{cm}$
- $|\text{Evt_bbcZ}| < 15\text{cm}$
- $1.2 < |\eta_{\text{FVTX}}| < 2.4$ for FVTX tracklets
- $|\eta_{\text{SVX}}| < 1$ for SVX tracklets

The run-averaged event multiplicity from South muon arm good runs are given in Fig. 8.

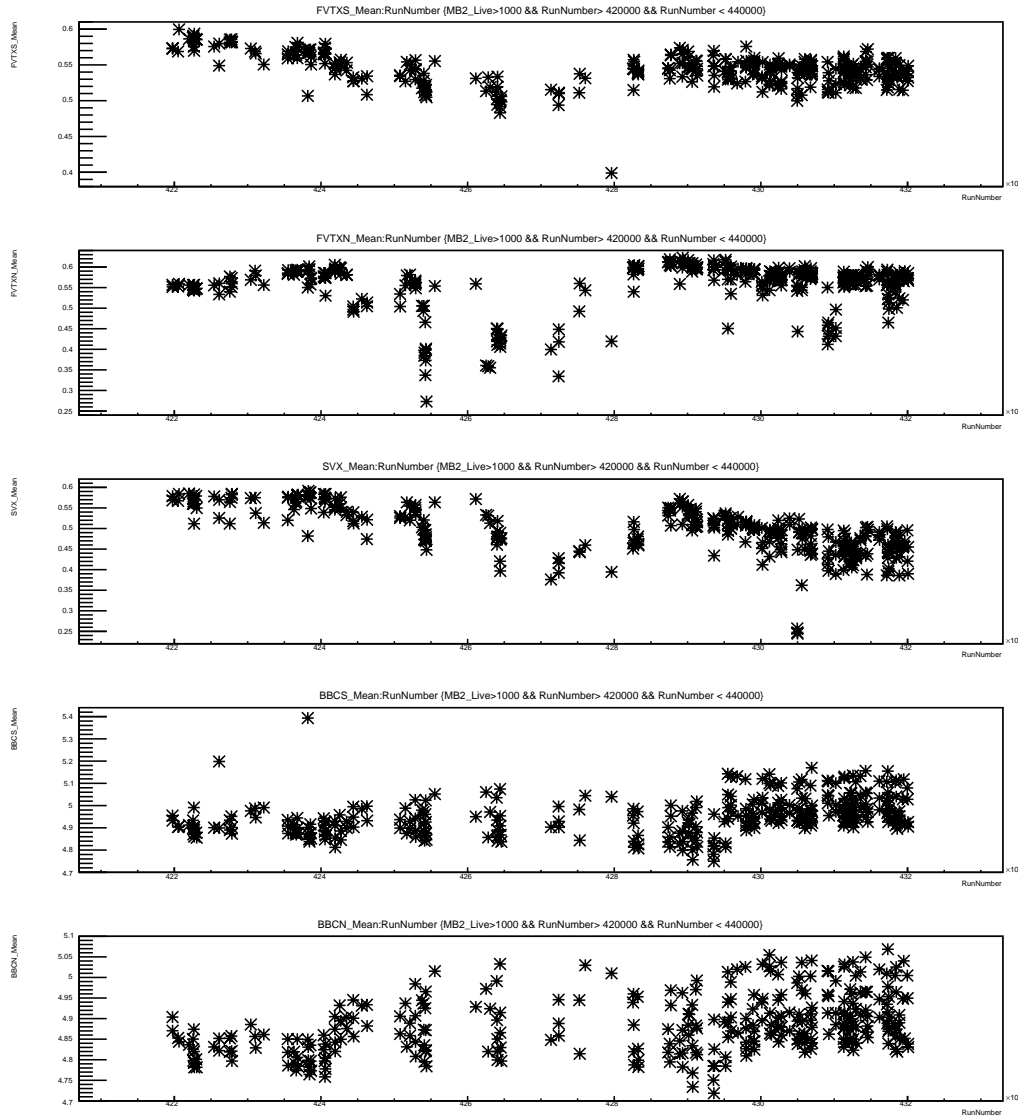


Figure 8: Run averaged $\text{Evt_Mult}_{(\text{FVTXS}, \text{FVTXN}, \text{SVX}, \text{BBCS}, \text{BBCN})}$ vs RunNumber from south-muon arm good run list.

The run-averaged event multiplicity from North muon arm good runs are given in Fig. 9. Any run with an average multiplicity beyond $\pm 20\%$ of the mean value are removed.

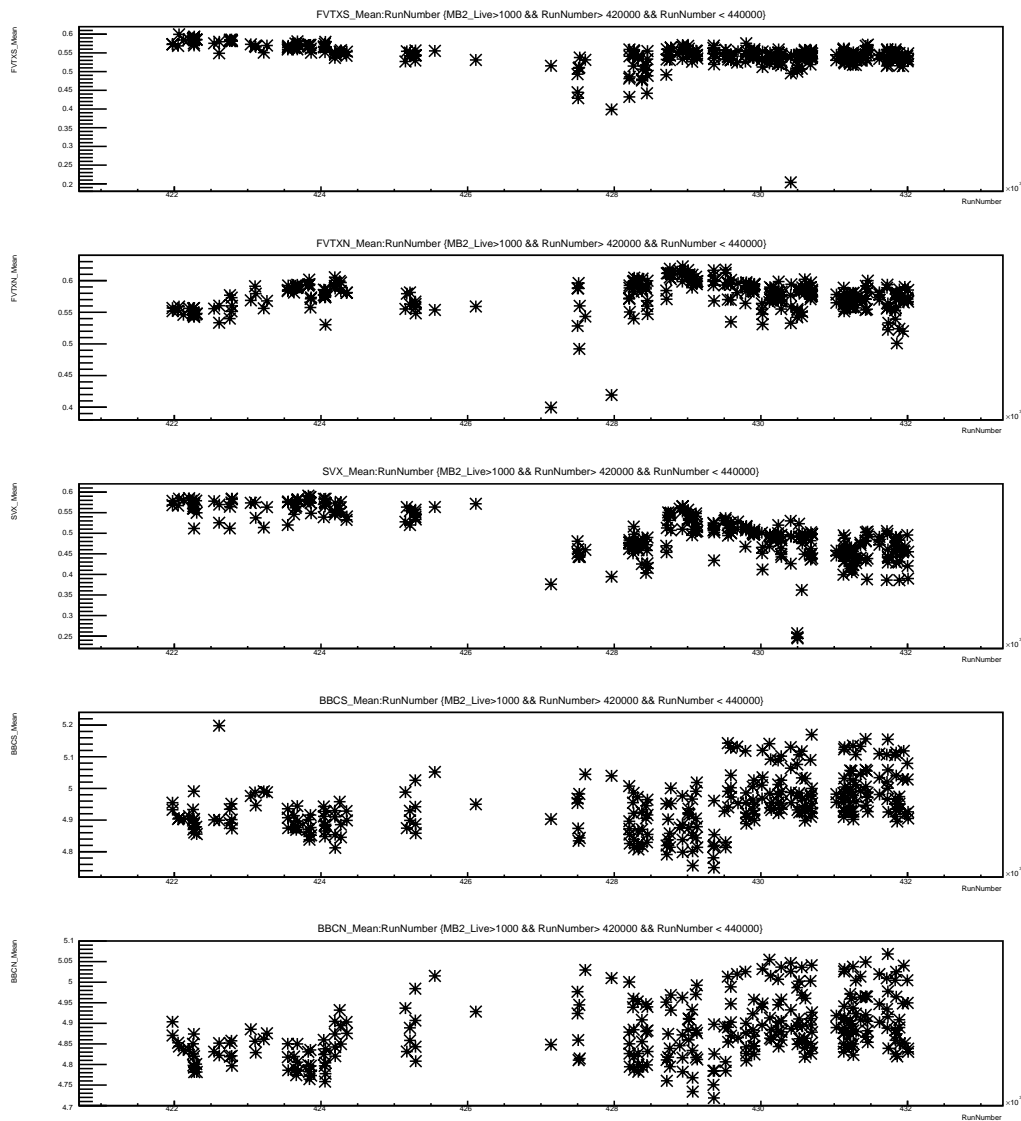


Figure 9: Run averaged Evt_Mult_(FVTXS, FVTXN, SVX, BBCS, BBCN) vs RunNumber from north-muon arm good run list.

4 Run15pp MB and Muon Data Analysis

There are two new unique experimental challenges in this analysis that we need to address carefully as they affect the event multiplicity distribution measurements:

- Skewed event multiplicity distributions due to multiple $p + p$ collisions at high luminosity in each beam crossing, see Fig. 10. This, in particular, enhances the event multiplicity distribution at high multiplicity, as shown later in Fig. 18
- Event trigger bias in BBCLL1 at high event multiplicities. Due to the finite acceptance of the PHENIX BBC detectors, events with a higher multiplicity tend to have higher probability to leave hits in both of the BBC detectors, leading to higher BBCLL1 trigger efficiency in $p + p$ collisions.

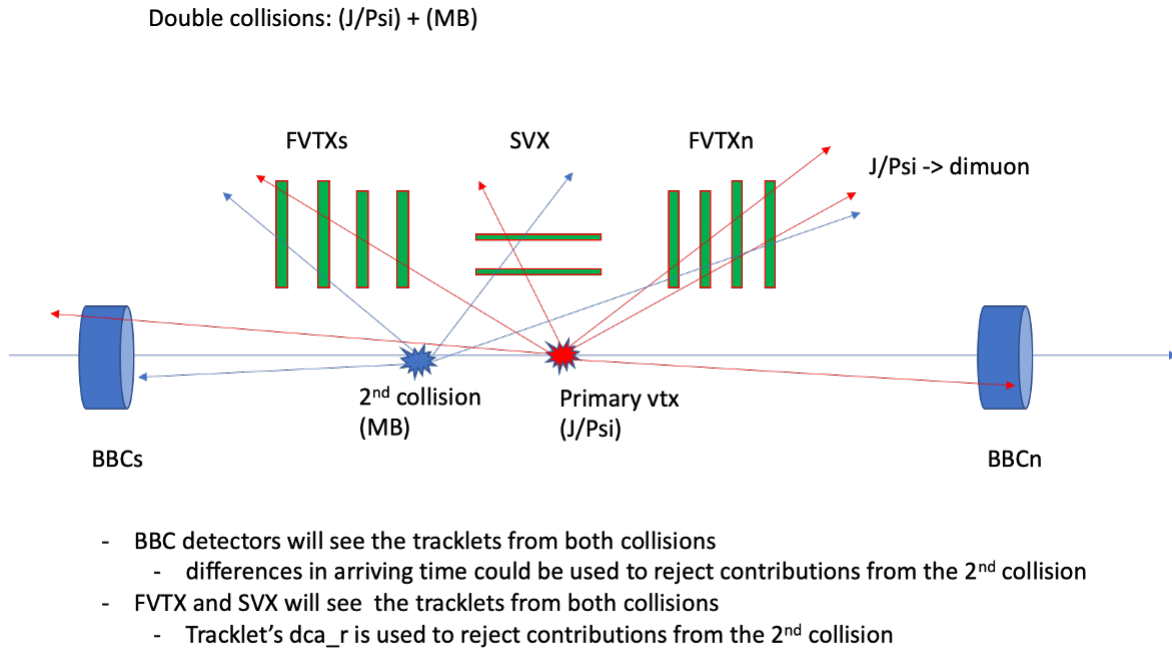


Figure 10: Double collisions in high luminosity $p + p$ run. The 2nd MB collision in a J/ψ event could contribute additional (background) tracklets in the FVTX and SVX tracklet reconstruction.

In the following, we will discuss the analysis techniques used to evaluate, minimize and correct such distortions in the measurements.

4.1 MB Event and FVTX and SVX tracklet selection

We use the reconstructed FVTX and SVX tracklets to classify the event multiplicity. To remove combinatorial background and have uniform tracklet acceptance, we use the following cuts to select events with well determined collision vertices:

- $|\text{Evt_vtxZ}| < 10\text{cm}$
- $|\text{Evt_bbcZ}| < 20\text{cm}$

Fig. 11 shows the MB event's z-vertex distributions as measured by the FVTX/SVX (Evt_vtxZ) and BBC (Evt_bbcZ). The vertex resolutions are about 0.5 mm for the FVTX/SVX z-vertex and 2 cm for the BBC one.

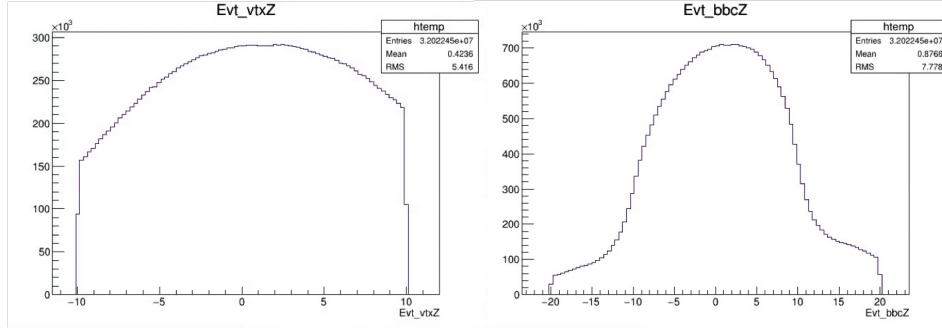


Figure 11: MB event z-vertex distributions reconstructed from silicon detectors (left: Evt_vtxZ) and from BBC (right: Evt_bbcZ), in cm.

Fig. 12 show the FVTX and SVS tracklets' DCA_r distributions, distance of the closest approach of the tracklet to the collision vertex.

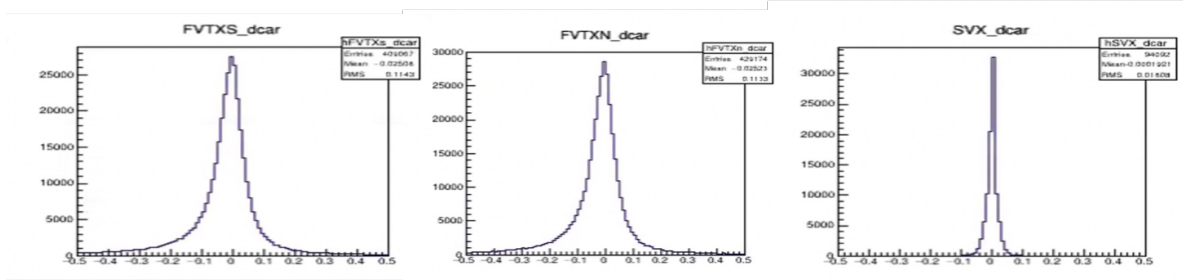


Figure 12: FVTXS, FVTXN and SVX tracklet's DCA_r distributions, in cm.

Due to finite detector sizes, FVTX and SVX acceptances depend on the collision vertex position. Fig. 13 show the FVTX and SVX tracklet's η distributions from $p+p$ collisions happened in 3 different vtxZ regions. The following cuts are used in the final analysis to select good FVTX and SVX tracklets in both MB and J/ψ events to minimize the collisions vertex dependence in the FVTX and SVX tracklet multiplicity measurements:

- $1.2 < |\eta_{\text{FVTX}}| < 2.4$ for FVTX tracklets
- $|\eta_{\text{SVX}}| < 1$ for SVX tracklets
- $\chi^2/\text{DOF} < 20$
- $\text{DCA}_r < 0.2$ cm for FVTX tracklets
- $\text{DCA}_r < 0.1$ cm for SVX tracklets

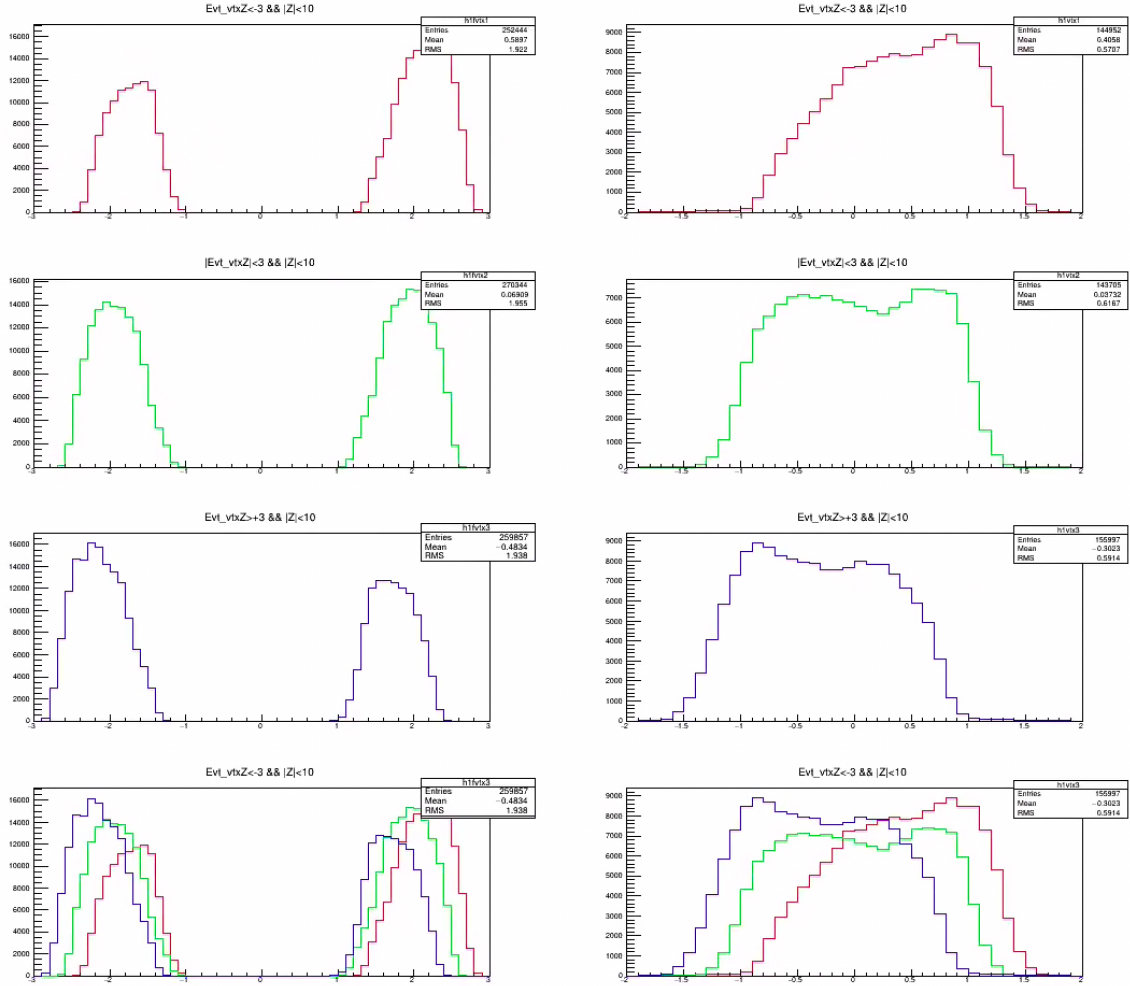


Figure 13: FVTX and SVX tracklet's η distributions in $p + p$ collisions in 3 Evt_vtxZ regions: (1) $-10 \text{ cm} < \text{Evt_vtxZ} < -3 \text{ cm}$ (top row), (2) $-3 \text{ cm} < \text{Evt_vtxZ} < +3 \text{ cm}$ (2nd row), (3) $+3 < \text{Evt_vtxZ} < +10 \text{ cm}$ (3rd row).

4.2 Run15pp Event Multiplicity Studies

After obtaining the signal raw yield, it is necessary to normalize them by the number of MB events. To obtain the number of MB events, we simply select the good runs from the MB dataset that is also in common with the dimuon trigger data to make sure we are looking at the same datasets. Then, we count the number of MB events in each multiplicity bin and scale them by the pre-scale factor run-by-run to obtain the number of MB events. There are three MB BBCLL1 triggers with loose online BBCz vertex cuts:

- MB0.Scale_Down: $|BBC_z| < 30$ cm (loose BBC z cut)
- MB1.Scale_Down: $|BBC_z| < \infty$ (no BBC z cut)
- MB2.Scale_Down: $|BBC_z| < 15$ cm (tight BBC z cut)

We use the MB2 triggered events in our analysis. We plot the FVTX North and South J/ψ events into the FVTXN, FVTXS, and SVX multiplicity bins [0,1,2,3,4,5,6,8,10,12,19]. Fig. 14 and Fig. 15 show the FVTX North and South MB events respectively.

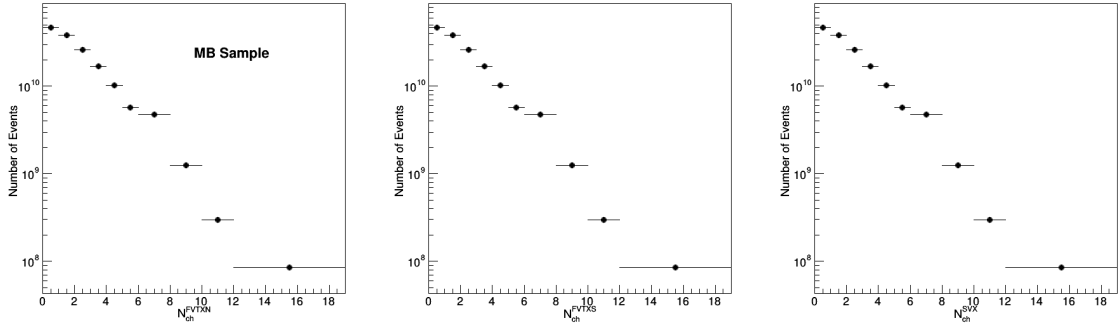


Figure 14: The number of FVTX North minimum biased events scaled by the prescale factor in good runs as a function of FVTXN, FVTXS, and SVX are shown above.

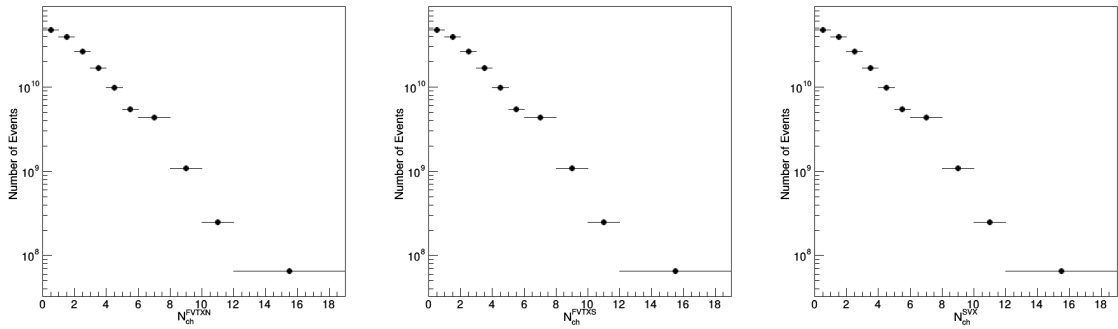


Figure 15: The number of FVTX South minimum biased events scaled by the prescale factor in good runs as a function of FVTXN, FVTXS, and SVX are shown above.

4.3 Multiple $p+p$ collisions and event multiplicity

One of the largest physics systematic uncertainties in the event multiplicity determination comes from the contributions of additional $p + p$ collisions beside the one that produces the J/ψ signal event as shown in Fig. 10. The big question is - what fraction of events at large event multiplicity are coming from double collisions? In the following, we use a data-driven method to estimate the contributions from multiple collisions.

Assuming Poisson statistics of the the beam-beam collisions at RHIC, one can estimate the average number of $p + p$ collisions per beam crossing, μ , from the measured BBC trigger rate and trigger efficiency,

$$R_{\text{BBC}}(\mu, \epsilon_{\text{NS}}, \epsilon_{\text{N}}, \epsilon_{\text{S}}) = f_{\text{RHIC}} \times [1 - e^{-\mu\epsilon_{\text{N}}} - e^{-\mu\epsilon_{\text{S}}} + e^{-\mu(\epsilon_{\text{N}} + \epsilon_{\text{S}} - \epsilon_{\text{NS}})}] \quad (5)$$

where $R_{\text{BBC}}(\mu, \epsilon_{\text{NS}}, \epsilon_{\text{N}}, \epsilon_{\text{S}})$ is the raw BBC(novtx) trigger rate, f_{RHIC} is the RHIC beam crossing rate (9.4MHz), $\epsilon_{\text{NS}}, \epsilon_{\text{N}}, \epsilon_{\text{S}}$ are the BBC trigger efficiencies of being hit in both(NS), North(N) and South(S) detectors, respectively. We quote the BBCLL1 trigger efficiency value of $\epsilon_{\text{NS}} = 55 \pm 5 \%$ from PPG228, and $\epsilon_{\text{S}} = \epsilon_{\text{N}} = \sqrt{\epsilon_{\text{NS}}}$. The derived BBCLL1 trigger rate vs the mean number of collision per beam-beam crossing is shown in Fig. 16.

In Run15pp, the maximum BBC rates are less than 2.5 MHz, as shown in Fig. 3, corresponding to less than 10 % of double collisions in the highest luminosity $p + p$ collisions, see Table 1. Given the average BBC rate of about 1000 kHz and the very low probability having more than 2 collisions per beam crossing, we only consider contributions from double collisions in the following discussions.

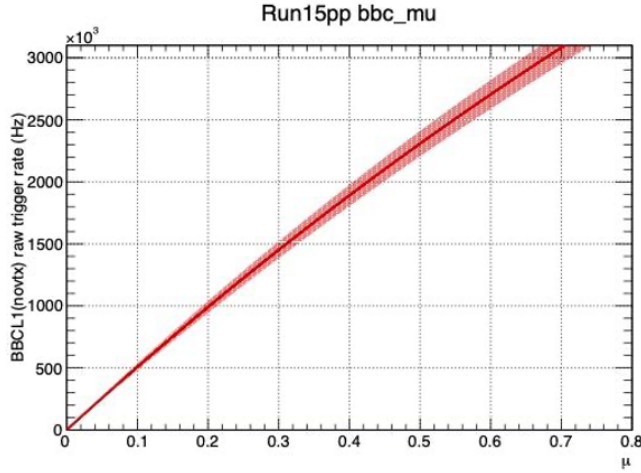


Figure 16: BBC rate vs average number of $p + p$ collisions μ . For Run15pp, the maximum BBC rate is less than 2.5 MHz, with averaged value around 800 kHz, corresponding to less than 2 % of double collision events.

To study the impact on the event-multiplicity determination from double collisions, we have developed a data driven method to estimate the contributions as a function of the measured event multiplicity N_{trk} . We derive the reference single collision events' multiplicity probability distribution function (PDF) $F_1(N_{\text{trk}})$ from the low collision rate MB runs, with BBC rate less than 500 kHz, where the double collision probability is less than 0.5 % and the contributions from the 2nd collision to the event multiplicity distribution is negligible. We calculate the double collision event track multiplicity distribution function $F_2(N_{\text{trk}})$ through the convolution:

$$F_2(N = N_1 + N_2) = F_1(N_1) \otimes F_1(N_2) \quad (6)$$

where N is the measured event multiplicity and N_1 and N_2 are the contributions from the first and second collisions, respectively. Fig. 17 shows the normalized PDF function constructed from low BBC

BBC Rate [kHz]	μ	Prob. of 2+ collisions	Prob. of 3+ collisions
250	0.05	0.12%	2.0×10^{-5}
500	0.10	0.47%	1.5×10^{-4}
800	0.16	1.2%	6.1×10^{-4}
1,000	0.20	1.8%	1.1×10^{-3}
1,200	0.24	2.5%	1.9×10^{-3}
1,500	0.31	3.9%	3.9×10^{-3}
1,800	0.36	5.1%	6.0×10^{-3}
2,000	0.43	6.9%	9.6×10^{-3}
2,500	0.55	10%	1.8×10^{-2}

Table 1: Probability of having more than one collisions per beam-beam crossing at a various BBCLL1 trigger rates. The mean BBC rate is about 1000 kHz in run15pp collisions.

rate runs, also shown (right) is the normalized multiplicity distribution from the events with clearly reconstructed 2nd collision vertex "Evt_vtxZ2", with $|Evt_vtxZ2| < 10$ cm.

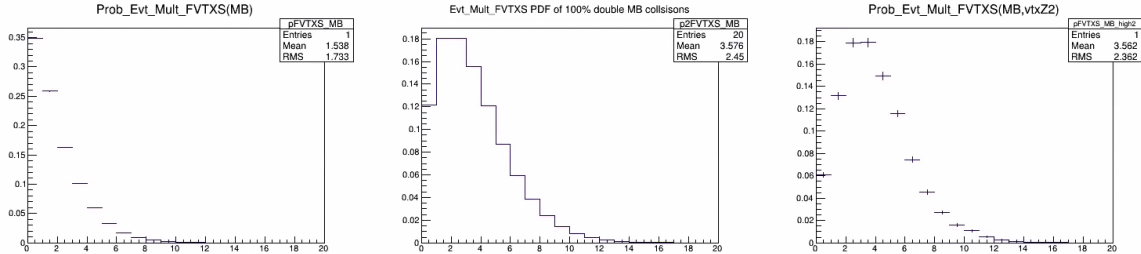


Figure 17: FVTXS event multiplicity probability distribution functions calculated from MB runs with BBC rate less than 500kHz: “single collision reference PDF $F_1(N_{\text{trk}})$ ” (left) and the derived double collision PDF $F_2(N_{\text{trk}})$ from Eq. 6 (middle), and PDF for double collision events with reconstructed 2nd vtxZ2 (right). The derived double collision PDF represents the real data reasonably well.

From above, we can derive the event multiplicity PDF for events that contain a fraction, x , of double collision events by:

$$F_x(N_{\text{trk}}) = (1 - x)F_1(N_{\text{trk}}) + xF_2(N_{\text{trk}}) \quad (7)$$

The correction factor for the event multiplicity for such events is given by,

$$R_{\text{double}}(N_{\text{trk}}, x) = \frac{F_x(N_{\text{trk}})}{F_1(N_{\text{trk}})} \quad (8)$$

We note the correction factor is most significant at large N_{trk} , as expected. Fig. 18 show an extreme case of 5 % mixture of double collisions in MB events (BBC Rate ~ 1.8 MHz).

To check the “single collision” assumption used in above calculations is reasonable, we also calculate the correction function for low BBC Rate events at 500 kHz using e.q. 7, with a double collision probability of about 0.5 %, see Fig. 19. We confirm the contribution from double collision is very small, less than 3 % at high FVTXS multiplicity of 10, much smaller than other systematic errors. We conclude runs with BBC rate less than 500 kHz are good samples of “single $p + p$ collisions”.

Additionally, we have also checked the ratio of the event multiplicity of data over the derived one with events that have clearly reconstructed second collision vertices beside the primary ones. Fig. 20 show the FVTX event multiplicity distributions from “double collision-like events” from data and “calculated double collisions PDF”, from Fig. 17. The maximum difference of about 20 % is quoted

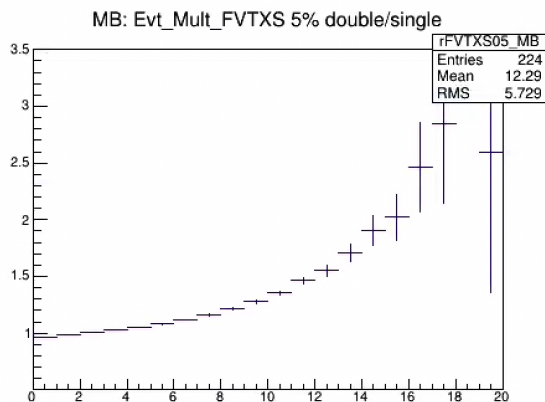


Figure 18: South FVTX event multiplicity PDF correction functions $R_x(N_{\text{trk}})$ for runs with 5% (corresponding to BBC Rate about 1.8MHz) double collision events.

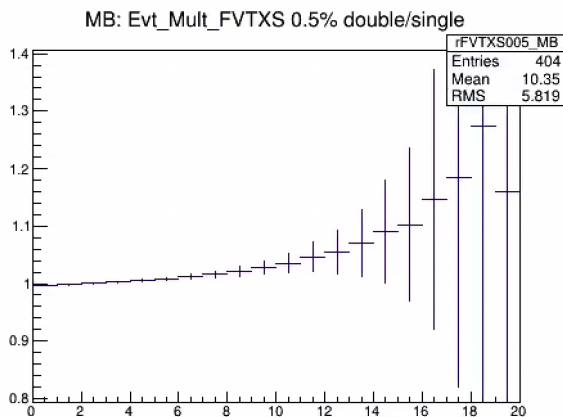


Figure 19: South FVTX event multiplicity PDF correction function $R_x(N_{\text{trk}})$ for runs with 0.5 % of double collisions (BBC Rate \sim 500 kHz). The correction factor is less than 3 % at high FVTXS multiplicity of 10, much less than other systematic corrections, i.e. they are a good sample of single $p + p$ collisions.

as systematic uncertainty for the time being. We note the second event vertices are often merged with the primary one in the event reconstruction if they are close in space, see Fig. 21. Thus we don't expect these two PDFs to be identical, further investigation will be carried out soon.

During the offline event collisions vertex reconstruction, if two vertices are very close, they have high probability to be merged as one. Fig. 20 shows the distribution of the distance between two reconstructed collision vertices, in cm.

Now we estimate the event multiplicity distribution correction factors. The luminosity averaged BBC rate is about 830 kHz as shown in above in Fig. 5, corresponding to than than 2 % of double collisions. The estimated correction function $R(N_{\text{trk}}, 2 \%)$ is shown in Fig. 22

We assign 20 % overall uncertainty as systematic error to the event multiplicity distributions.

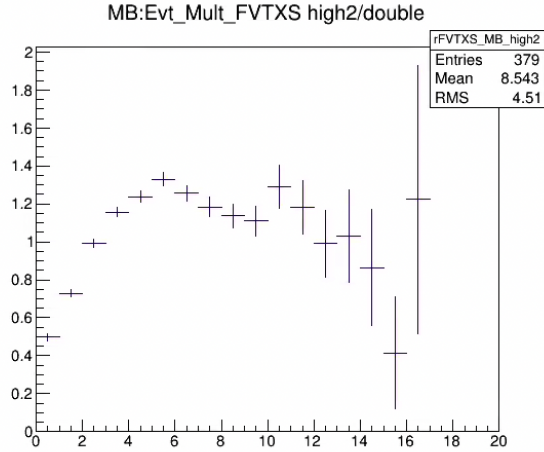


Figure 20: Ratio of the FVTXS multiplicity distribution of events with two collision vertices ($|Evt_vtxZ| < 10$ cm and $|Evt_vtxZ2| < 10$ cm) over calculated double collision PDF. We assign the 20 % difference as a systematic uncertainty in the multiplicity correction factor.

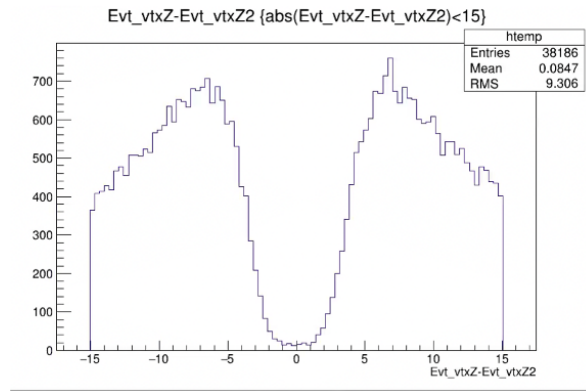


Figure 21: Difference between two reconstructed collision vertices Evt_vtxZ and Evt_vtxZ2 in $p + p$ collisions (in cm). Two vertices are often merged into one if they are very close in space.

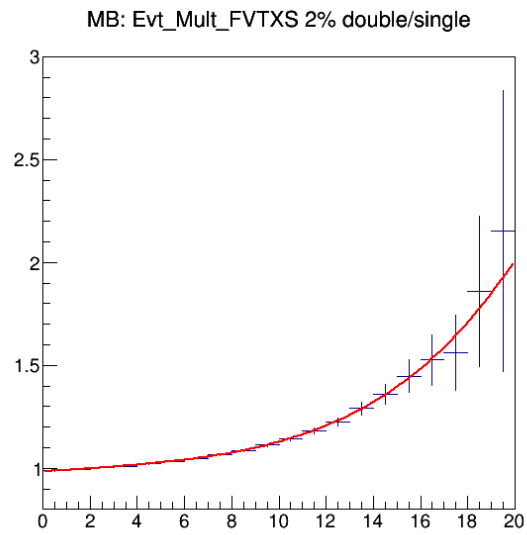


Figure 22: FVTX South multiplicity distribution correction function for MB events. Less than 2 % of double collisions are in the total sample. The correction factor is less than 5 % at FVTX South multiplicity of 10.

4.4 Run15pp MB Trigger bias analysis

In PHENIX, we used BBC detectors to identify the MB $p + p$ collisions, BBCLL1 trigger. Since BBC detectors had limited acceptance in the forward region only, ($3.1 < |\eta| < 3.7$), an event with higher multiplicity tends to have higher probability to be triggered by BBCLL1, and such bias must be corrected in the analysis.

The average BBCLL1 trigger efficiency is $55 \pm 5 \%$ for MB and $79 \pm 2 \%$ for hard scattering like J/ψ events from previous run15 pp dimuon J/ψ resolution (PPG224), [1]. For our physics study, we also need the event multiplicity dependent BBCLL1 trigger efficiency.

We have developed a data-driven method to estimate the trigger bias correction by using RHIC beam-clock triggered data. Fig. 23 shows the triggers used in run15pp run, for Run number 430238. During run15pp run, we consistently took beam-clock triggered data at a rate of about 50 Hz.

Trigger

Note: LI Trigger Scaler Entries in pink indicate an approximate count due to the fact that Run Control may have crashed and the run was not ended properly.
select * from trigger where runnumber = 430238 order by binb

Name	Bit Mask	Scale Down	State	Raw Trigger Count	Raw Trigger Rate	Live Trigger Count	Live Trigger Rate	Scaled Trigger Count	Scaled Trigger Rate	Livetime
BBCLL1(>0 tubes)	0x00000001	6050	Enabled	1639647284	631362.07	1516649492	584000.57	250644	96.51	0.92
BBCLL1(>0 tubes) novertex	0x00000002	10890	Enabled	3140094215	1209123.69	2904883029	1118553.34	266724	102.70	0.93
ZDCLL1wide	0x00000004	215	Enabled	37431042	14413.19	34852564	13420.32	161355	62.13	0.93
BBCLL1(noVtx)&(ZDCNI ZDCS)	0x00000008	497	Enabled	352021148	135549.15	327730370	126195.75	658093	253.41	0.93
BBCLL1(>0 tubes) narrowvtx	0x00000010	684	Enabled	623960338	240261.97	577145076	222235.30	842547	324.43	0.92
ZDCNS	0x00000020	215	Enabled	41603160	16019.70	38517046	14831.36	178320	68.66	0.93
ERT_4x4b	0x00000040	0	Enabled	325323	125.27	290981	112.05	290981	112.05	0.89
ERT_4x4a&BBCLL1	0x00000080	0	Enabled	1898429	731.01	1754389	675.54	1754389	675.54	0.92
ERT_4x4c&BBCLL1(narrow)	0x00000100	1	Enabled	2503685	964.07	2316076	891.83	1158038	445.91	0.93
ERTLL1_E&BBCLL1(narrow)	0x00000200	0	Enabled	290927	112.02	270425	104.13	270425	104.13	0.93
FVTX_HighMult_N_AND_S&BBCLL1narrow	0x00000400	0	Enabled	165410	63.69	154173	59.37	154173	59.37	0.93
FVTX_HighMult_N_OR_S&BBCLL1narrow	0x00000800	3	Enabled	3597816	1385.37	3352323	1290.84	838081	322.71	0.93
MPC_N_S_A	0x00001000	0	Enabled	6477479	2494.22	5866231	2258.85	5866231	2258.85	0.91
MPC_S_B	0x00002000	0	Enabled	1352815	520.91	1240069	477.50	1240069	477.50	0.92
MPC_S_C&ERTLL1_2x2	0x00004000	0	Enabled	57337	22.08	53289	20.52	53289	20.52	0.93
MPC_S_C&MPC_S_C	0x00008000	0	Enabled	19200	7.39	17585	6.77	17585	6.77	0.92
CLOCK	0x00100000	196077	Enabled	24373510209	9385256.15	22555985894	8685400.81	115035	44.30	0.93
MPC_N_B	0x00200000	0	Enabled	1826481	703.30	1660558	639.41	1660558	639.41	0.91
MPC_N_C&ERTLL1_2x2	0x00040000	0	Enabled	68936	26.54	63695	24.53	63695	24.53	0.92
MPC_N_C&MPC_N_C	0x00080000	0	Enabled	31227	12.02	23656	9.11	23656	9.11	0.76
MUIDLL1_N2D&BBCLL1novtx	0x00100000	0	Enabled	46081	17.74	31809	12.25	31809	12.25	0.69
MUIDLL1_S2D&BBCLL1novtx	0x00200000	0	Enabled	31864	12.27	20358	7.84	20358	7.84	0.64
MUIDLL1_N1D&BBCLL1novtx	0x00400000	18	Enabled	6752076	2599.95	6140067	2364.29	323161	124.44	0.91
MUIDLL1_S1D&BBCLL1novtx	0x00800000	9	Enabled	3616460	1392.55	3313542	1275.91	331354	127.59	0.92
MUON_N_SG3&MUIDLL1_(ID IH)&BBCLL1novtx(nppg)	0x01000000	0	Enabled	1852279	713.24	1605051	618.04	1605051	618.04	0.87
MUON_N_SG3&MUIDLL1_(ID IH)&BBCLL1novtx(nppg)	0x02000000	0	Enabled	487995	187.91	432284	166.46	432284	166.46	0.89
MUON_N_SG3&BBCLL1novtx(nppg)	0x04000000	615	Enabled	188772815	72688.80	175224907	67472.05	284456	109.53	0.93
MUON_N_SG3&BBCLL1novtx(nppg)	0x08000000	107	Enabled	29541804	11375.36	27306331	10514.57	252836	97.36	0.92
PPG(Pedestal)	0x10000000	0	Enabled	2583	0.99	2457	0.95	2457	0.95	0.95
PPG(Test Pulse)	0x20000000	0	Enabled	5167	1.99	4906	1.89	4906	1.89	0.95
PPG(Laser)	0x40000000	0	Enabled	5167	1.99	4889	1.88	4889	1.88	0.95
Noise	0x80000000	0	Disabled	45023360	17336.68	0	0.00	0	0.00	0.00

Figure 23: Run15pp trigger configuration from Run number 430238. We took beam-clock triggered data at about 44.3Hz

From beam-clock triggered data, we declare that a collision happened if there is at least one tracklet in the FVTX or SVX. The BBCLL1 efficiency vs FVTX (SVX) multiplicity is given by,

$$\epsilon(N_{\text{trk}}) = \frac{FVTX(N_{\text{trk}}) \& \& BBCLL1}{FVTX(N_{\text{trk}})} \quad (9)$$

We have also studied the event multiplicity dependent BBCLL1 trigger bias corrections for low and high BBC rates runs:

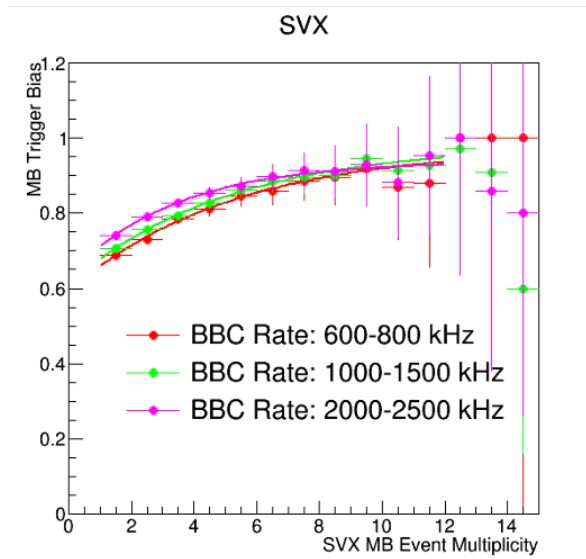


Figure 24: BBCLL1 trigger bias correction factor vs event multiplicity, for $p + p$ collisions in 3 distinct BBC rates.

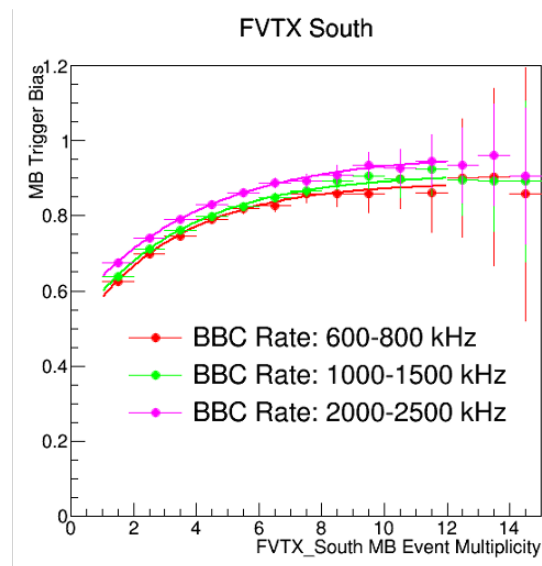


Figure 25: BBCLL1 trigger bias correction factor vs event multiplicity, for $p + p$ collisions in 3 distinct BBC rates.

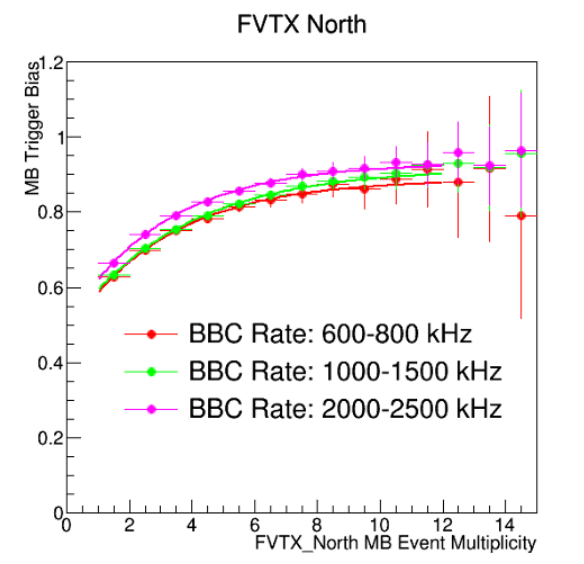


Figure 26: BBCLL1 trigger bias correction factor vs event multiplicity, for $p + p$ collisions in 3 distinct BBC rates.

4.5 p+p MU analysis: J/ψ Signal Extraction

J/ψ signals are extracted from the dimuon triggered data, from MUIDLL1_N2D_BBCLL1(novtx) and MUIDLL1_S2D_BBCLL1(novtx).

To obtain the J/ψ signal raw yield $N^{J/\psi}$ in the dimuon triggered datasets, we need to extract it from the $\mu^+\mu^-$ invariant mass distribution. In our analysis, we fit to the unbinned data sample to extract the J/ψ signal raw yield. We use the *RooFit* package, which is an analysis module based on the ROOT framework dedicated for nuclear and high-energy physics. The details of *RooFit* can be found at: <https://root.cern/manual/roofit/>

In our analysis, we use the a double Crystal Ball function (CB) to model the signal [2]. Its functional form for the signal component is shown below:

$$f(m_{J/\psi}; \alpha, n, \mu, \sigma) = \begin{cases} N \exp[-\frac{(x-\mu)^2}{2\sigma^2}], & \text{if } (\frac{x-\mu}{\sigma} > \alpha) \\ NA(B - \frac{x-\mu}{\sigma})^{-n} & \text{if } (\frac{x-\mu}{\sigma} \leq \alpha) \end{cases} \quad (10)$$

The signal component is a linear combination of two Crystal Ball functions.

$$F_s = kCB_1 + (1 - k)CB_2 \quad (11)$$

where $0 < k < 1$.

For the background, we fit it with an exponential function. Its functional form is shown below:

$$F_B(m_{J/\psi}; D, \lambda) = De^{(-\lambda m_{J/\psi})} \quad (12)$$

The total fitting function F to be fitted to the data is the sum of the signal and background with signal yield, S , and background yield, B , as the parameter to be extracted:

$$F = S \cdot F_s + B \cdot F_B \quad (13)$$

We will fit the function F to the dimuon invariant mass of the dimuon trigger sample and evaluate the S and B from the data to extract the signal raw yield $N^{J/\psi}$ and its uncertainty by imposing a signal mass window $|m_{\mu\mu} - m_{J/\psi}| < 0.4 \text{ GeV}/c^2$.

The fit performance as well as the J/ψ signal raw yield of each multiplicity bin of [0,1,2,3,4,5,6,8,10,12,19] with respect FVTXN, FVTXS, and SVX are show respectively in Figure 27, 35 and Table 4.5, 6 below:

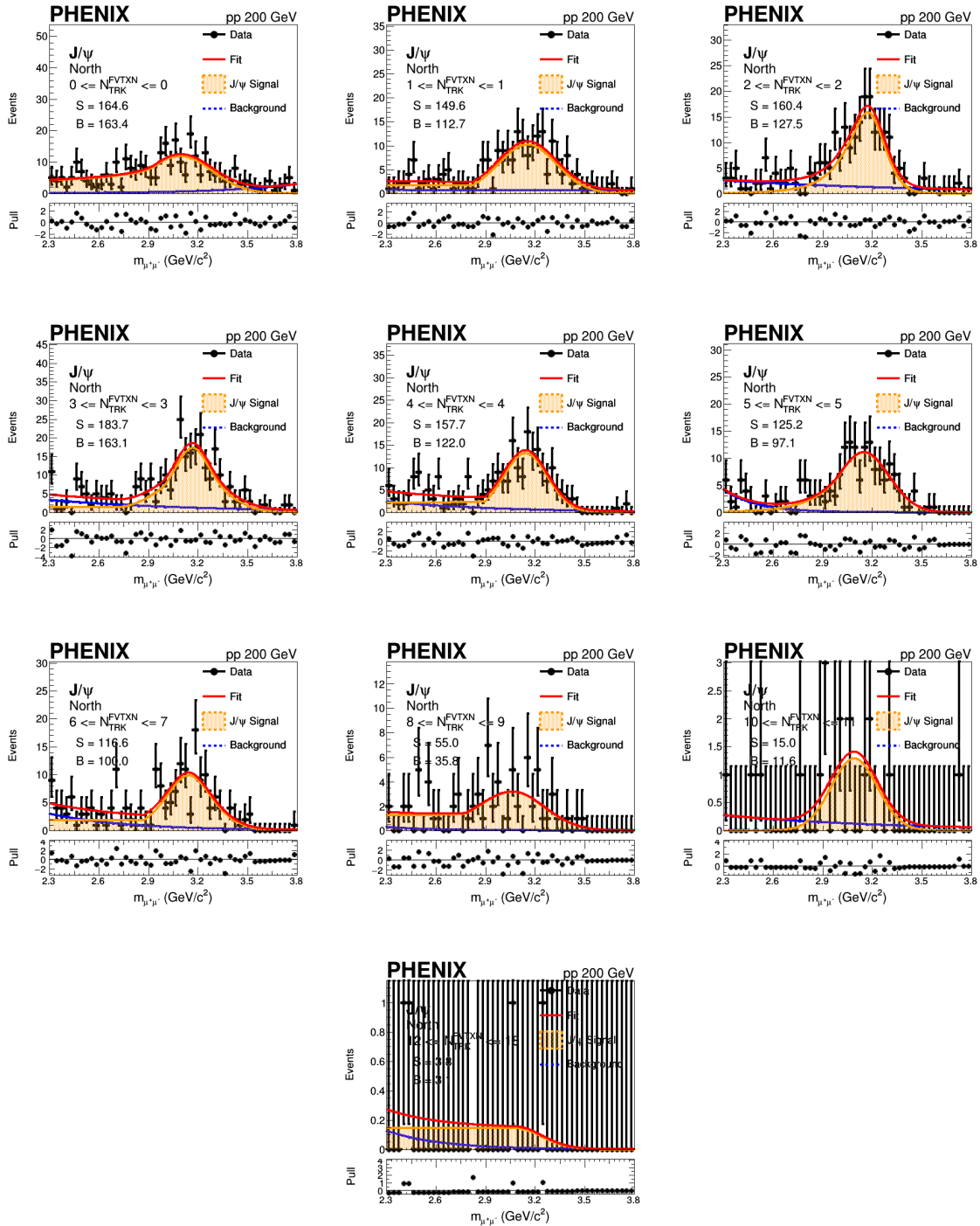


Figure 27: The unbinned fits to the dimuon invariant mass distributions of dimuon triggered sample to obtain the J/ψ invariant mass from the North FVTX Arm for each North FVTX multiplicity bin are shown above.

FVTXN Multiplicity	$N^{J/\psi}$	μ (GeV/c ²)	σ (GeV/c ²)
0 - 1	164.6 ± 27.7	3.092 ± 0.025	0.194 ± 0.036
1 - 2	149.6 ± 37.3	3.154 ± 0.021	0.120 ± 0.240
2 - 3	160.4 ± 16.7	3.172 ± 0.022	0.093 ± 0.021
3 - 4	183.7 ± 80.3	3.167 ± 0.022	0.087 ± 0.036
4 - 5	157.7 ± 36.8	3.142 ± 0.014	0.133 ± 0.059
5 - 6	125.2 ± 10.2	3.150 ± 0.014	0.153 ± 0.011
6 - 8	116.6 ± 30.9	3.145 ± 0.019	0.095 ± 0.101
8 - 10	55.0 ± 10.4	3.063 ± 0.042	0.188 ± 0.116
10 - 12	15.0 ± 4.4	3.092 ± 0.041	0.140 ± 0.099
12 - 19	3.8 ± 0.0	3.080 ± 0.037	0.000 ± 0.000

Table 2: Summary of FVTXN J/ψ signal raw yield $N^{J/\psi}$, mean μ , and width σ for each FVTXN multiplicity bin.

Figure 34 plots the fitting parameters signal raw yield $N^{J/\psi}$, mean μ , and width σ for each FVTXN multiplicity bin

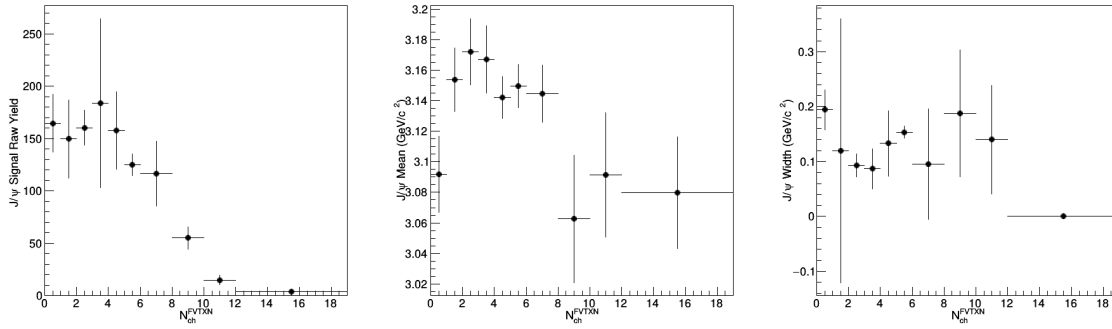


Figure 28: The signal raw yield $N^{J/\psi}$, mean μ , and width σ from the unbinned fit to the J/ψ invariant mass distribution as a function of FVTX North multiplicity are shown above.

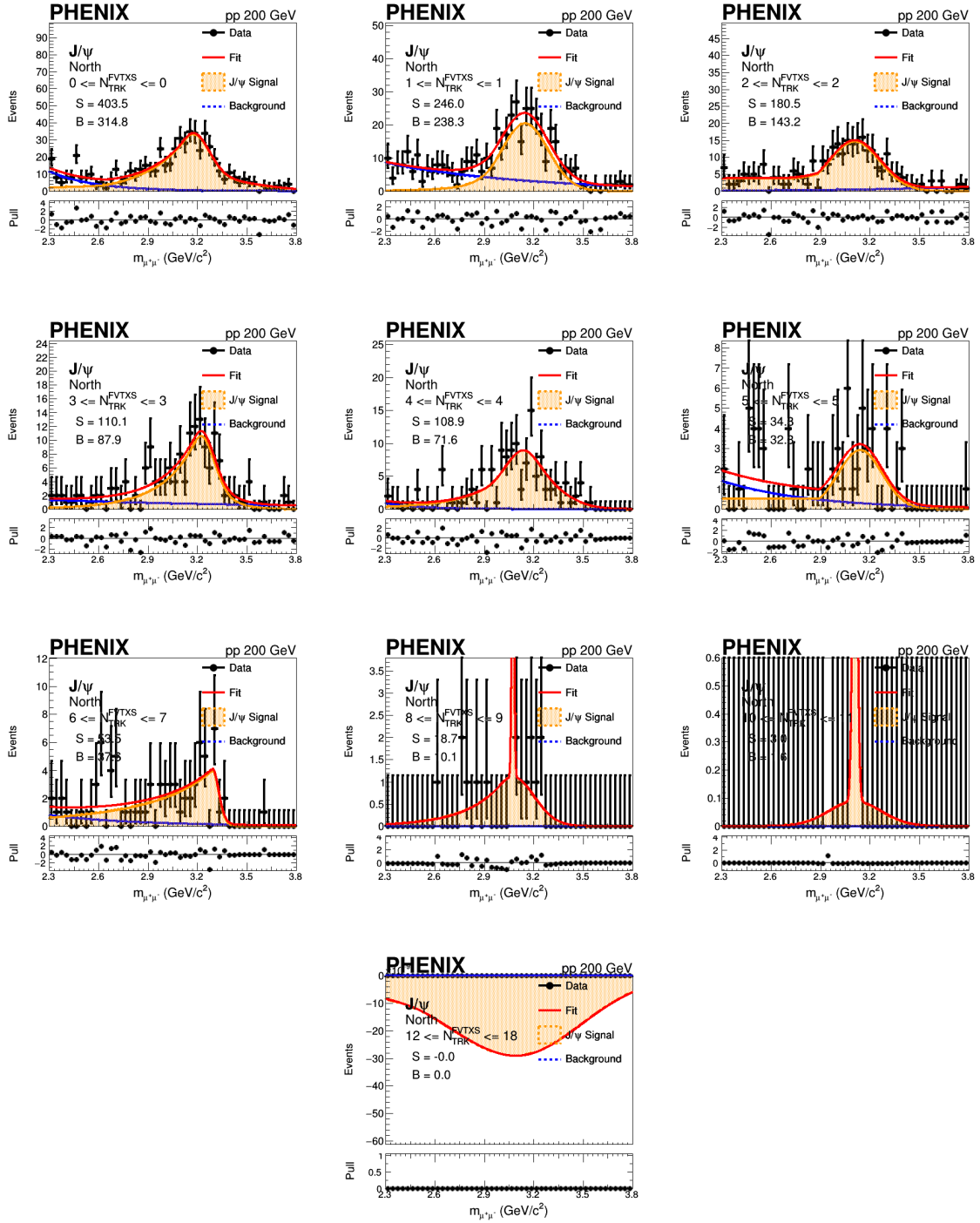


Figure 29: The unbinned fits to the dimuon invariant mass distributions of dimuon triggered sample to obtain the J/ψ invariant mass from the North FVTX Arm for each South FVTX multiplicity bin are shown above.

Table 3: Summary of FVTXN J/ψ signal raw yield $N^{J/\psi}$, mean μ , and width σ for each FVTXN multiplicity bin.

FVTXN Multiplicity	$N^{J/\psi}$	μ (GeV/c ²)	σ (GeV/c ²)
0 - 1	403.5 ± 39.4	3.176 ± 0.023	0.097 ± 0.028
1 - 2	246.0 ± 36.1	3.148 ± 0.013	0.146 ± 0.053
2 - 3	180.5 ± 26.4	3.107 ± 0.015	0.156 ± 0.143
3 - 4	110.1 ± 18.2	3.222 ± 0.023	0.080 ± 0.027
4 - 5	108.9 ± 12.7	3.137 ± 0.016	0.086 ± 0.052
5 - 6	34.8 ± 12.4	3.141 ± 0.030	0.137 ± 0.253
6 - 8	53.5 ± 8.3	3.294 ± 0.011	0.023 ± 0.441
8 - 10	18.7 ± 4.3	3.075 ± 0.004	0.007 ± 0.003
10 - 12	3.0 ± 1.0	3.110 ± 0.006	0.014 ± 0.004
12 - 19	-0.0 ± 0.2	3.090 ± 0.168	0.400 ± 0.337

Figure 36 plots the fitting parameters signal raw yield $N^{J/\psi}$, mean μ , and width σ for each FVTXN multiplicity bin

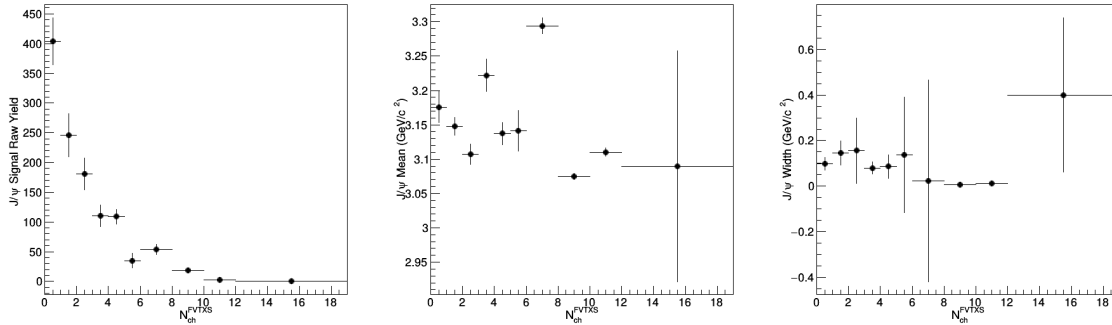


Figure 30: The signal raw yield $N^{J/\psi}$, mean μ , and width σ from the unbinned fit to the J/ψ invariant mass distribution as a function of FVTX South multiplicity are shown above.

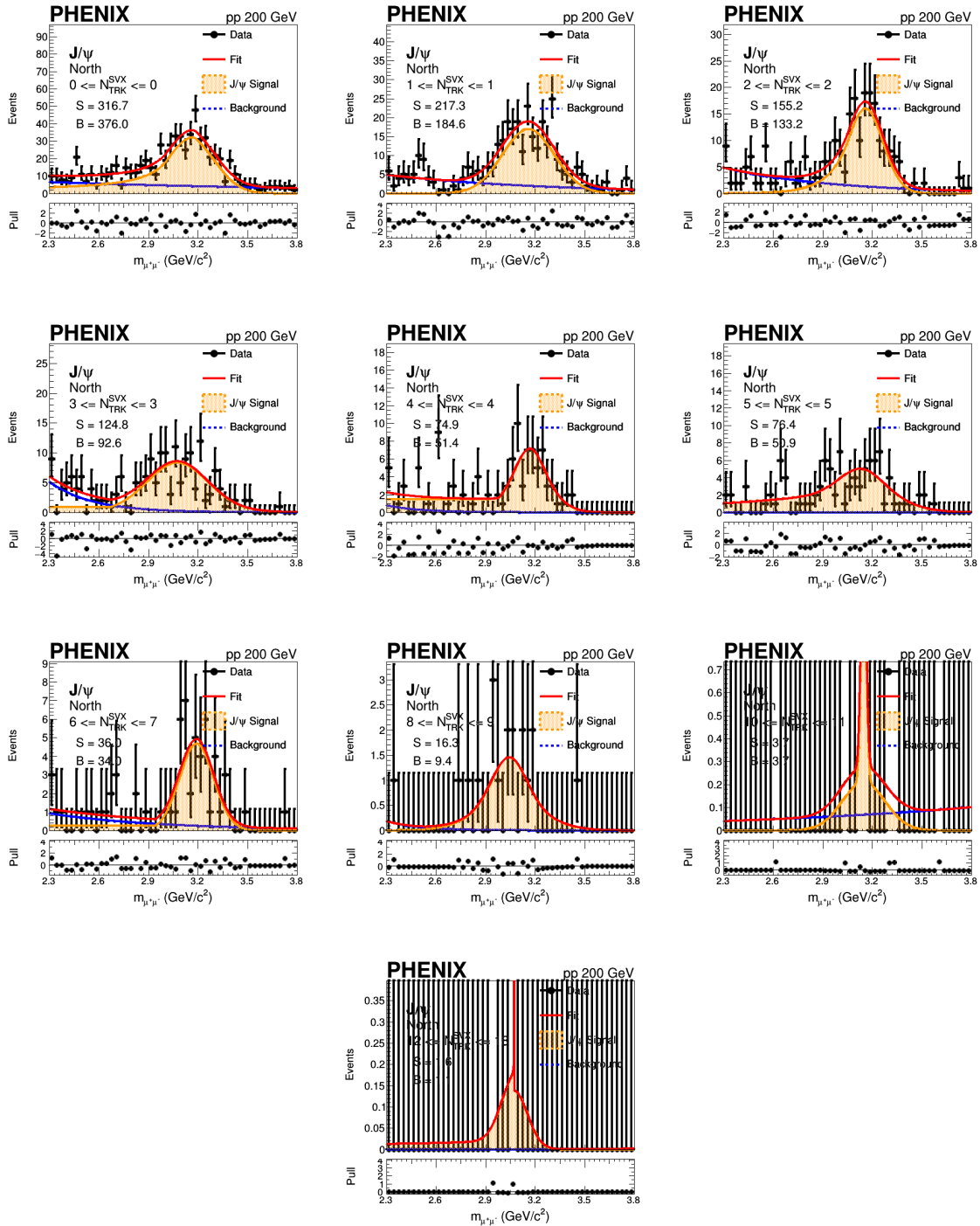


Figure 31: The unbinned fits to the dimuon invariant mass distributions of dimuon triggered sample to obtain the J/ψ invariant mass from the North FVTX Arm for each SVX multiplicity bin are shown above.

Table 4: Summary of FVTXN J/ψ signal raw yield $N^{J/\psi}$, mean μ , and width σ for each FVTXN multiplicity bin.

FVTXN Multiplicity	$N^{J/\psi}$	μ (GeV/c ²)	σ (GeV/c ²)
0 - 1	316.7 ± 45.4	3.165 ± 0.057	0.143 ± 0.010
1 - 2	217.3 ± 19.7	3.159 ± 0.013	0.157 ± 0.037
2 - 3	155.2 ± 2.2	3.159 ± 0.002	0.108 ± 0.026
3 - 4	124.8 ± 24.1	3.076 ± 0.026	0.307 ± 0.635
4 - 5	74.9 ± 9.3	3.168 ± 0.017	0.076 ± 0.033
5 - 6	76.4 ± 7.8	3.125 ± 0.037	0.132 ± 0.048
6 - 8	36.0 ± 9.2	3.192 ± 0.015	0.104 ± 0.434
8 - 10	16.3 ± 4.0	3.044 ± 0.037	0.204 ± 0.055
10 - 12	3.7 ± 2.3	3.148 ± 0.016	0.016 ± 0.009
12 - 19	1.6 ± 0.0	3.074 ± 0.000	0.000 ± 0.617

Figure 38 plots the fitting parameters signal raw yield $N^{J/\psi}$, mean μ , and width σ for each SVX multiplicity bin

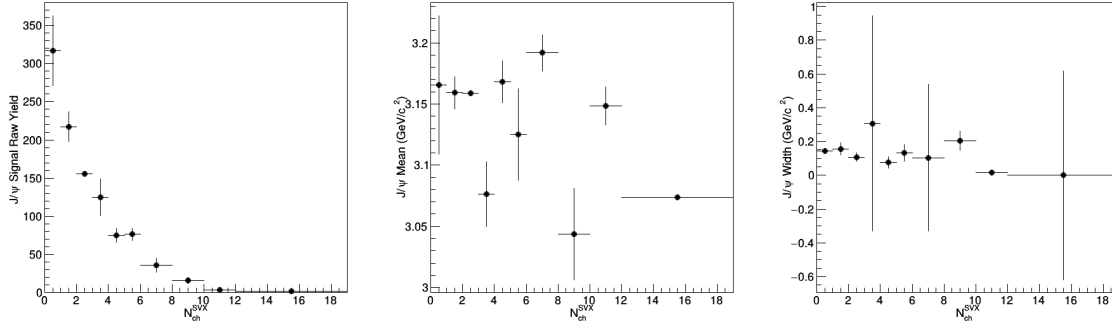


Figure 32: The signal raw yield $N^{J/\psi}$, mean mass μ , and width σ from the unbinned fit to the J/ψ invariant mass distribution as a function of SVX multiplicity are shown above.

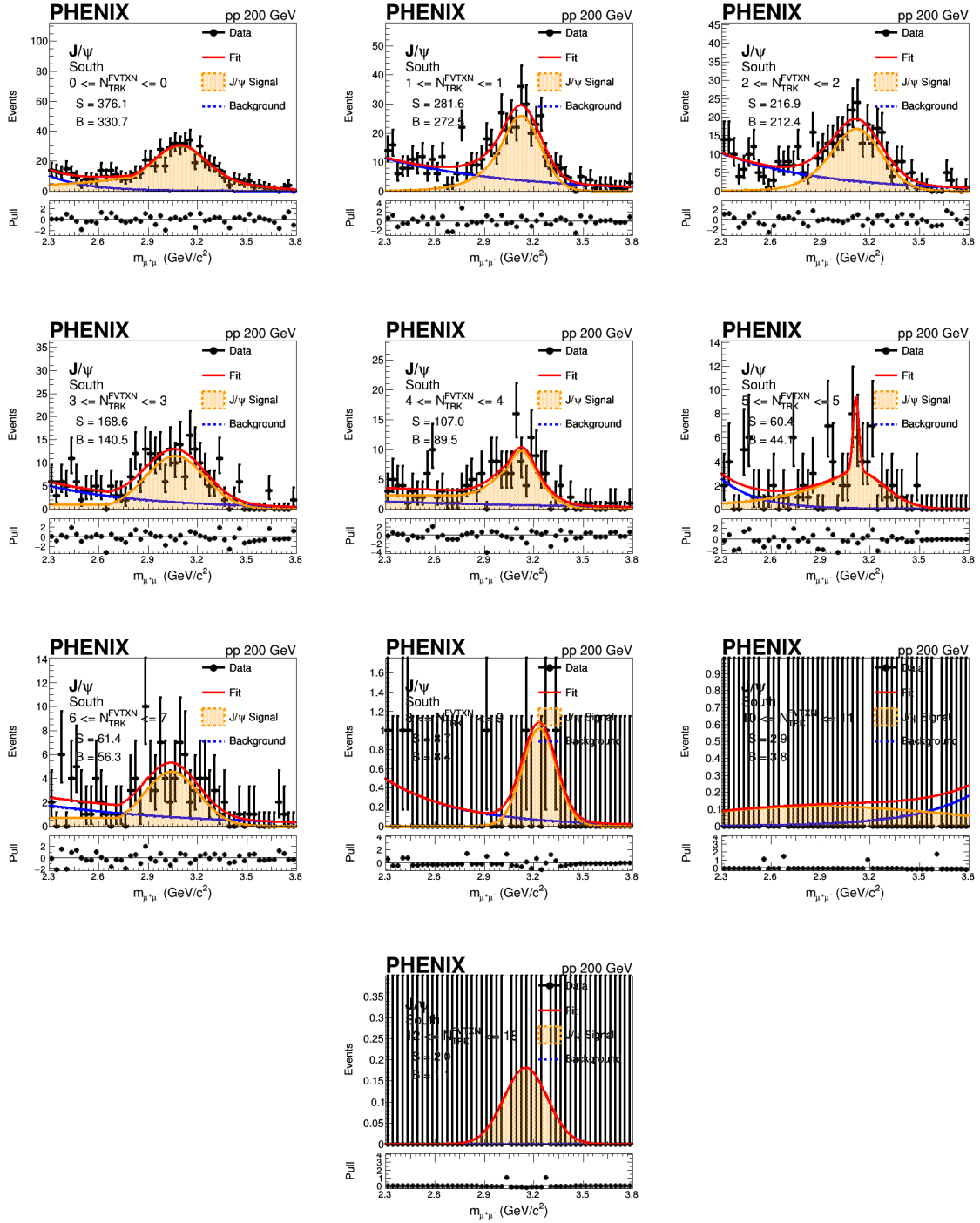


Figure 33: The unbinned fits to the dimuon invariant mass distributions of dimuon triggered sample to obtain the J/ψ invariant mass from the South FVTX Arm for each North FVTX multiplicity bin are shown above.

FVTXN Multiplicity	$N^{J/\psi}$	μ (GeV/c ²)	σ (GeV/c ²)
0 - 1	376.1 ± 16.5	3.095 ± 0.010	0.153 ± 0.009
1 - 2	281.6 ± 38.6	3.124 ± 0.057	0.095 ± 0.588
2 - 3	216.9 ± 24.1	3.119 ± 0.020	0.134 ± 0.042
3 - 4	168.6 ± 23.9	3.066 ± 0.019	0.174 ± 0.278
4 - 5	107.0 ± 66.5	3.124 ± 0.036	0.074 ± 0.049
5 - 6	60.4 ± 37.8	3.116 ± 0.010	0.017 ± 0.008
6 - 8	61.4 ± 17.4	3.043 ± 0.030	0.176 ± 0.279
8 - 10	8.7 ± 3.6	3.235 ± 0.051	0.175 ± 0.278
10 - 12	2.9 ± 1.4	2.900 ± 0.333	0.563 ± 0.515
12 - 19	2.0 ± 1.1	3.152 ± 0.071	0.135 ± 0.496

Table 5: Summary of FVTXN J/ψ signal raw yield $N^{J/\psi}$, mean μ , and width σ for each FVTXN multiplicity bin.

Figure 34 plots the fitting parameters signal raw yield $N^{J/\psi}$, mean μ , and width σ for each FVTXN multiplicity bin

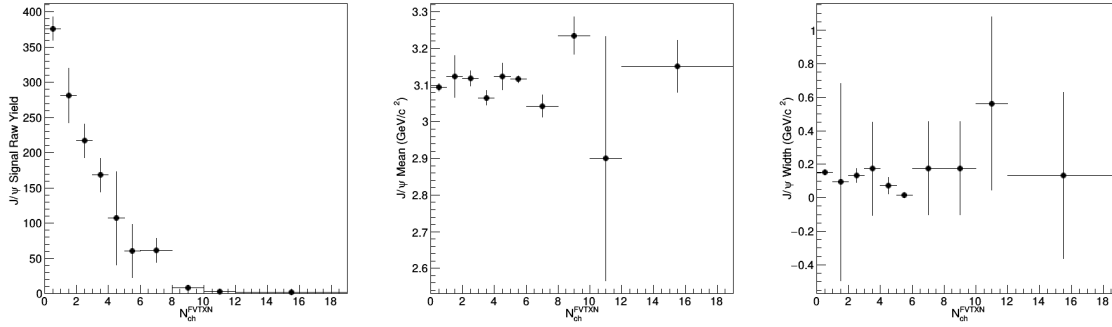


Figure 34: The signal raw yield $N^{J/\psi}$, mean μ , and width σ from the unbinned fit to the J/ψ invariant mass distribution as a function of FVTX North multiplicity are shown above.

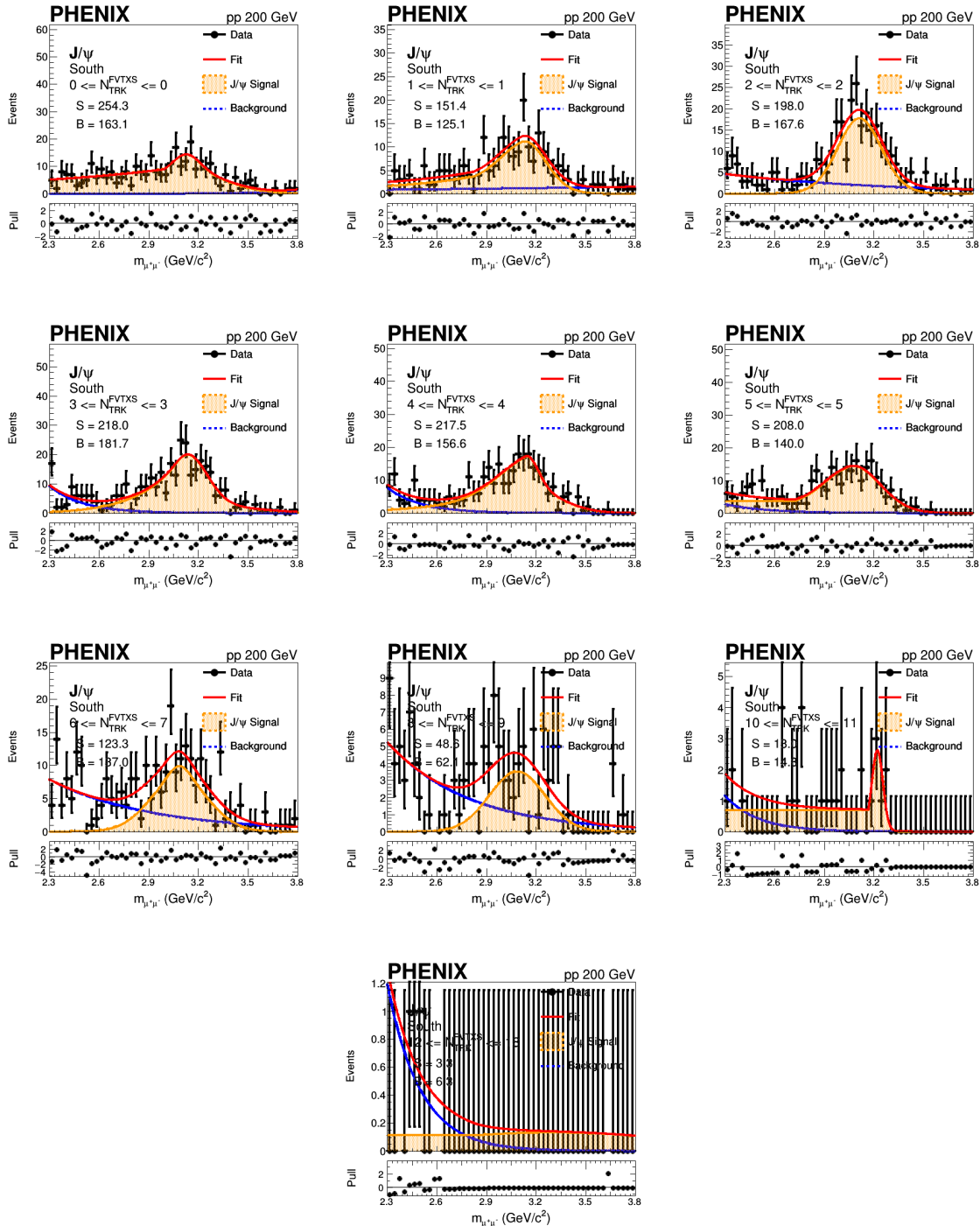


Figure 35: The unboxed fits to the dimuon invariant mass distributions of dimuon triggered sample to obtain the J/ψ invariant mass from the South FVTX Arm for each South FVTX multiplicity bin are shown above.

Table 6: Summary of FVTXN J/ψ signal raw yield $N^{J/\psi}$, mean μ , and width σ for each FVTXN multiplicity bin.

FVTXN Multiplicity	$N^{J/\psi}$	μ (GeV/c ²)	σ (GeV/c ²)
0 - 1	254.3 ± 14.0	3.126 ± 0.019	0.084 ± 0.021
1 - 2	151.4 ± 53.3	3.132 ± 0.035	0.145 ± 0.050
2 - 3	198.0 ± 15.5	3.114 ± 0.012	0.113 ± 0.028
3 - 4	218.0 ± 13.2	3.137 ± 0.012	0.117 ± 0.011
4 - 5	217.5 ± 14.1	3.145 ± 0.013	0.069 ± 0.013
5 - 6	208.0 ± 25.7	3.077 ± 0.031	0.139 ± 0.122
6 - 8	123.3 ± 18.7	3.086 ± 0.023	0.063 ± 0.058
8 - 10	48.6 ± 11.0	3.087 ± 0.034	0.150 ± 0.195
10 - 12	18.0 ± 1.4	3.222 ± 0.005	0.037 ± 0.767
12 - 19	3.3 ± 1.6	3.300 ± 0.307	0.678 ± 0.497

Figure 36 plots the fitting parameters signal raw yield $N^{J/\psi}$, mean μ , and width σ for each FVTXN multiplicity bin

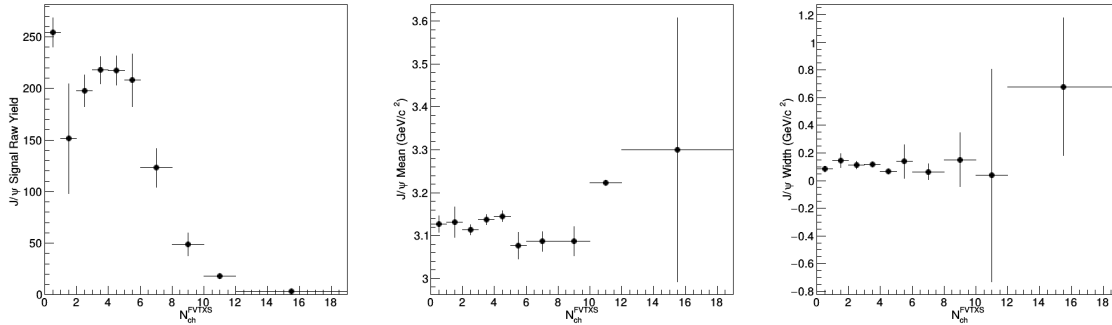


Figure 36: The signal raw yield $N^{J/\psi}$, mean μ , and width σ from the unbinned fit to the J/ψ invariant mass distribution as a function of FVTX South multiplicity are shown above.

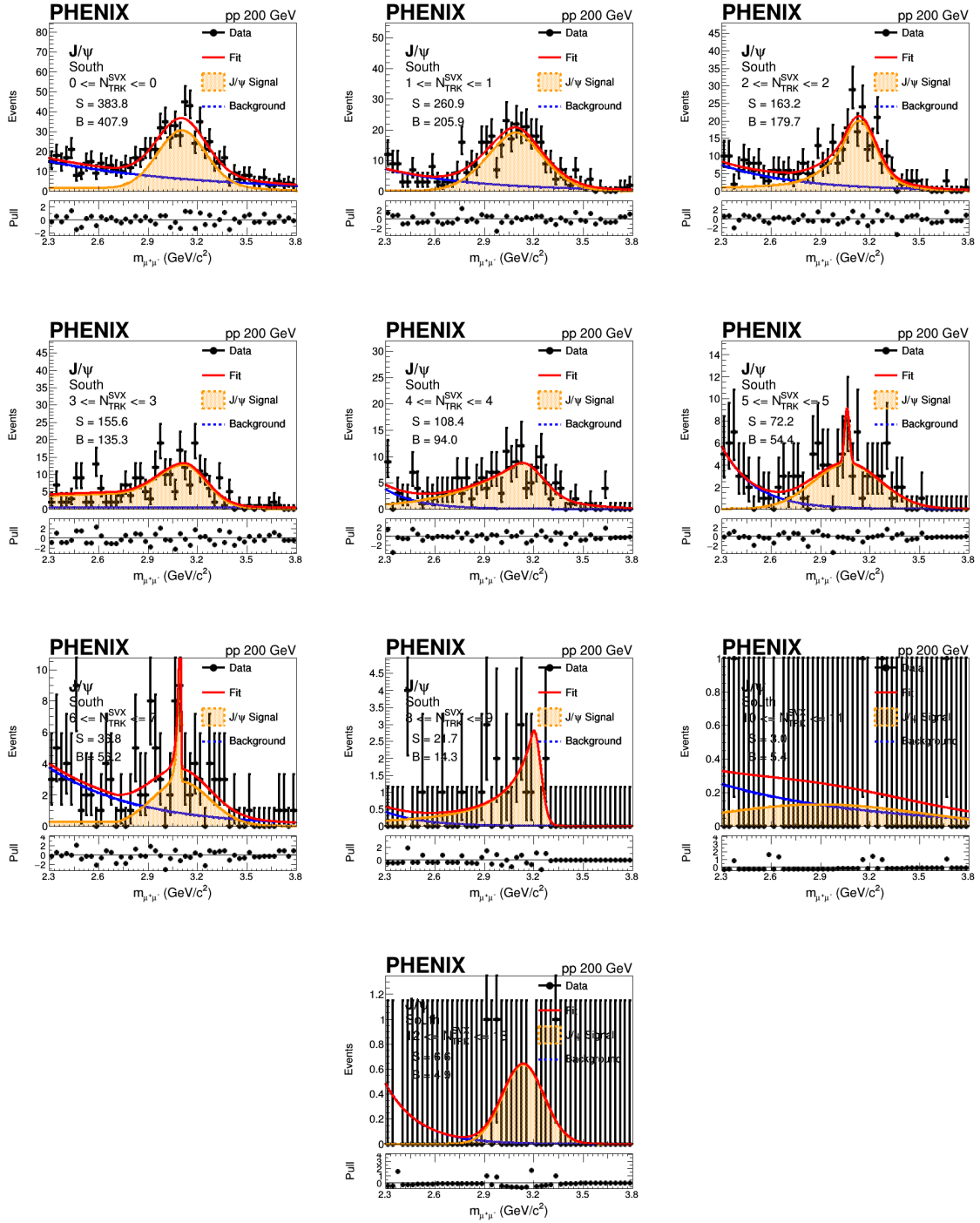


Figure 37: The unbinned fits to the dimuon invariant mass distributions of dimuon triggered sample to obtain the J/ψ invariant mass from the South FVTX Arm for each SVX multiplicity bin are shown above.

Table 7: Summary of FVTXN J/ψ signal raw yield $N^{J/\psi}$, mean μ , and width σ for each FVTXN multiplicity bin.

FVTXN Multiplicity	$N^{J/\psi}$	μ (GeV/c ²)	σ (GeV/c ²)
0 - 1	383.8 \pm 81.1	3.105 \pm 0.011	0.144 \pm 0.023
1 - 2	260.9 \pm 24.8	3.090 \pm 0.022	0.093 \pm 0.057
2 - 3	163.2 \pm 35.4	3.135 \pm 0.014	0.098 \pm 0.017
3 - 4	155.6 \pm 14.2	3.116 \pm 0.051	0.151 \pm 0.023
4 - 5	108.4 \pm 8.9	3.131 \pm 0.020	0.126 \pm 0.018
5 - 6	72.2 \pm 8.6	3.062 \pm 0.010	0.206 \pm 0.021
6 - 8	36.8 \pm 9.4	3.099 \pm 0.002	0.003 \pm 0.002
8 - 10	21.7 \pm 7.6	3.203 \pm 0.019	0.069 \pm 0.418
10 - 12	3.0 \pm 1.9	2.900 \pm 0.245	0.589 \pm 0.453
12 - 19	6.6 \pm 1.7	3.137 \pm 0.033	0.127 \pm 0.023

Figure 38 plots the fitting parameters signal raw yield $N^{J/\psi}$, mean μ , and width σ for each SVX multiplicity bin

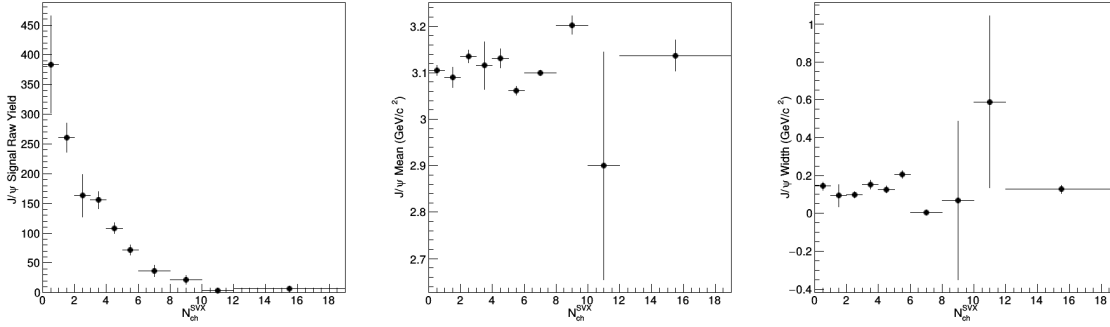


Figure 38: The signal raw yield $N^{J/\psi}$, mean μ , and width σ from the unbinned fit to the J/ψ invariant mass distribution as a function of SVX multiplicity are shown above.

We could see that the fits look very nice and the J/ψ signal raw yields look reasonable. We will use the $N^{J/\psi}$ as the signal raw yield to evaluate \hat{r} .

4.6 Closure Test of Unbinned Fit

The last step of signal extraction is to test its closure. To make sure our fits are valid, we produce 1000 MC toy samples based on the data and fit each of the sample with our model. Then, we plot the parameter, parameter error, and the pull distributions. We finally fit the pull distribution with a Gaussian function. If our fits have good closure, we should see the Gaussian fits to the pull distributions to have a width near 1 and mean near 0, which we call unity pull.

Figure 39, 40, 41, 42, 43, and 44 below show the pull distributions as well as the Gaussian fits for North FVTX J/ψ and South J/ψ for each FVTXN, FVTXS, and SVX bin:

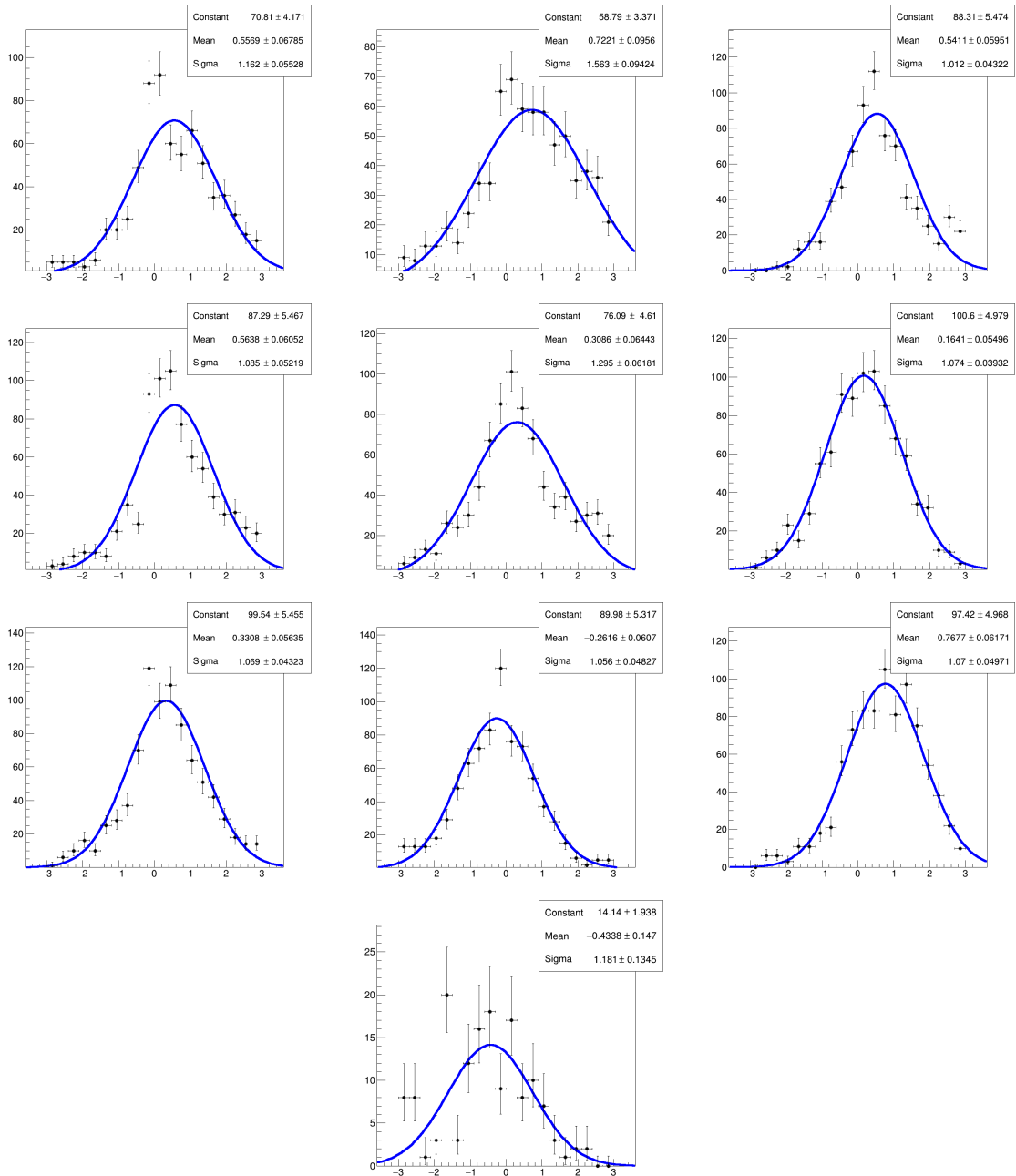


Figure 39: The closure test of FVTX North J/ψ for each FVTXN multiplicity bin is shown above. We can see overall unity pull for most of the pull distributions.

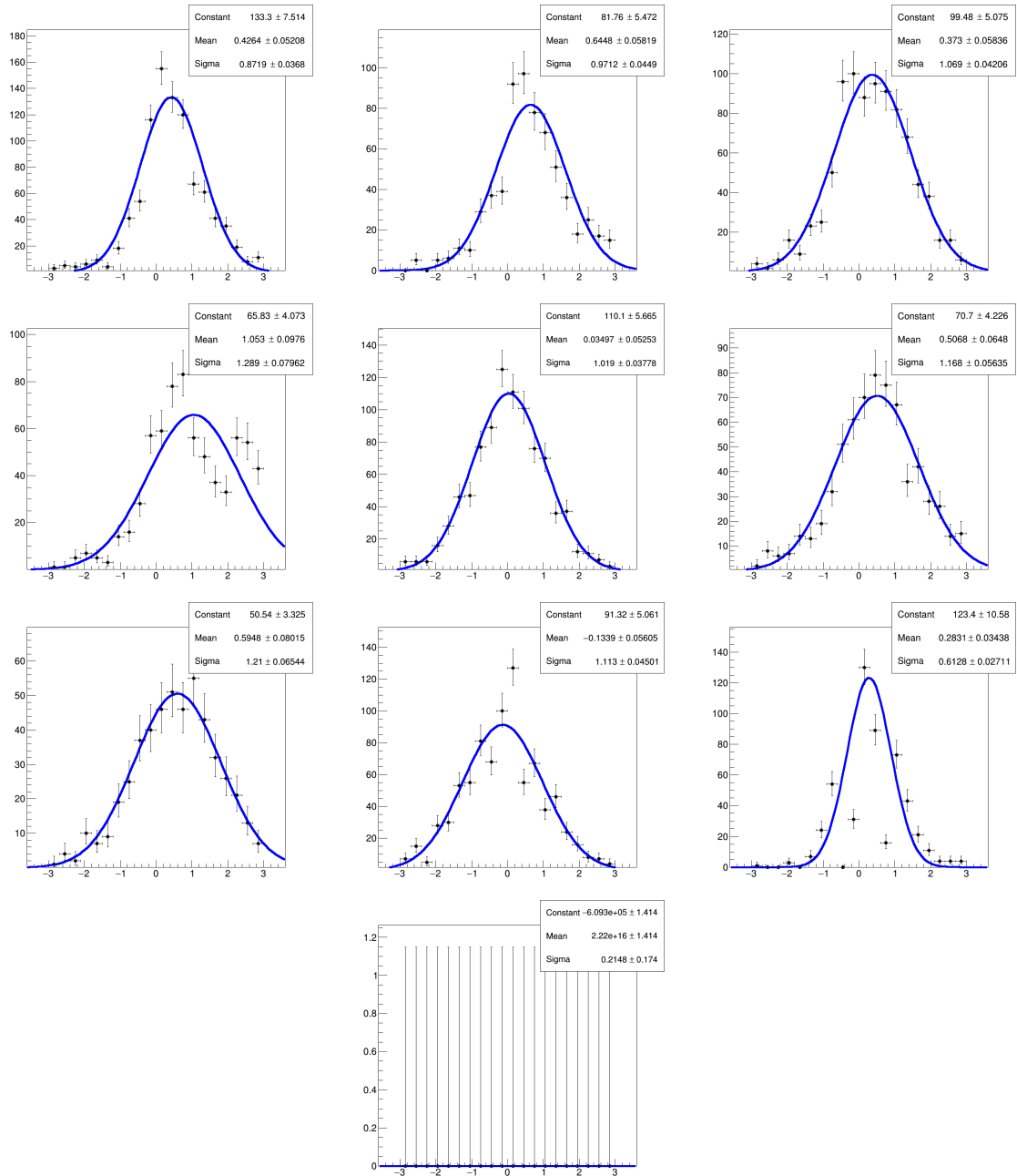


Figure 40: The closure test of FVTX North J/ψ for each FVTXS multiplicity bin is shown above. We can see overall unity pull for most of the pull distributions.

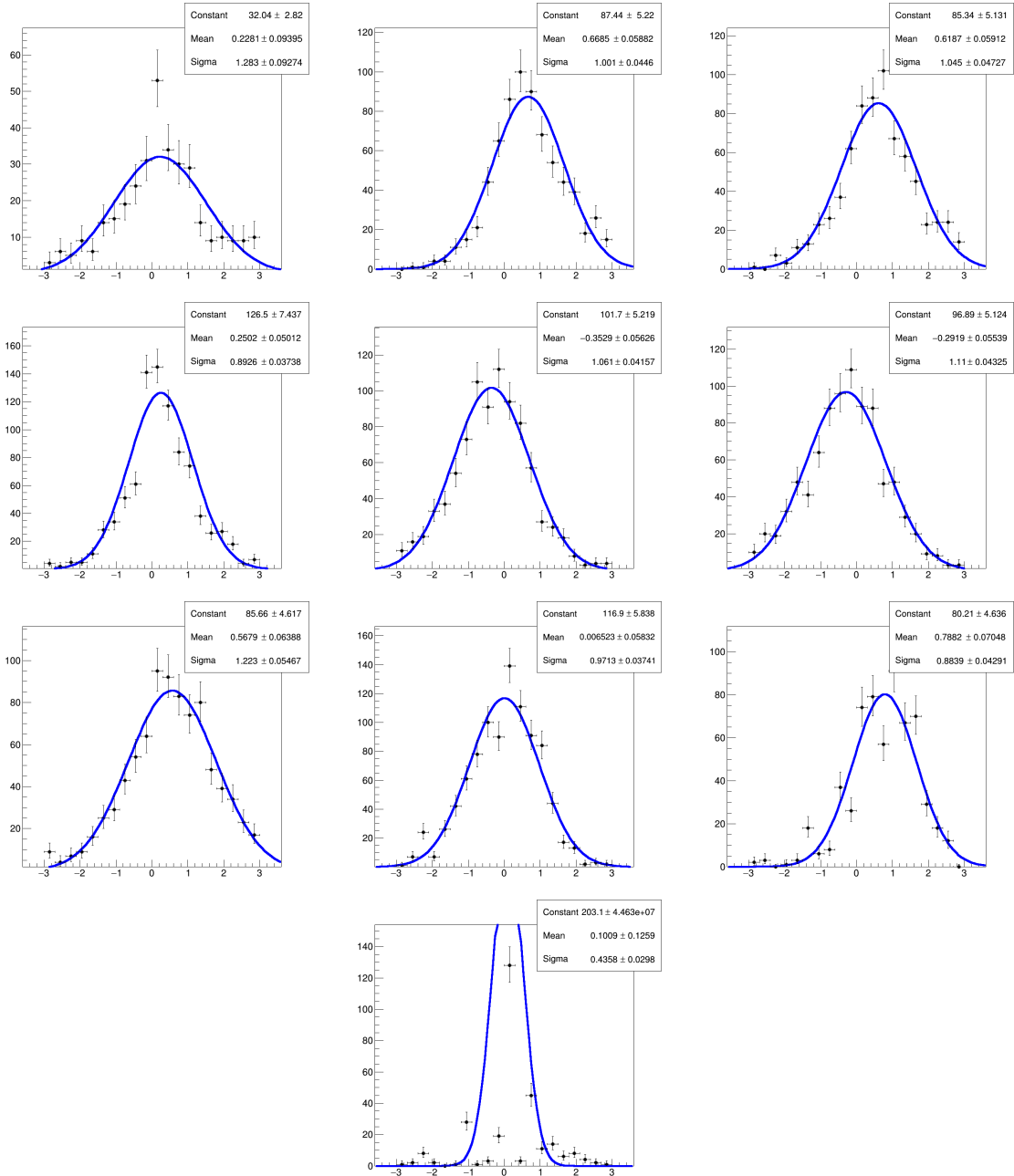


Figure 41: The closure test of FVTX North J/ψ for each FVTXS multiplicity bin is shown above. We can see overall unity pull for most of the pull distributions.

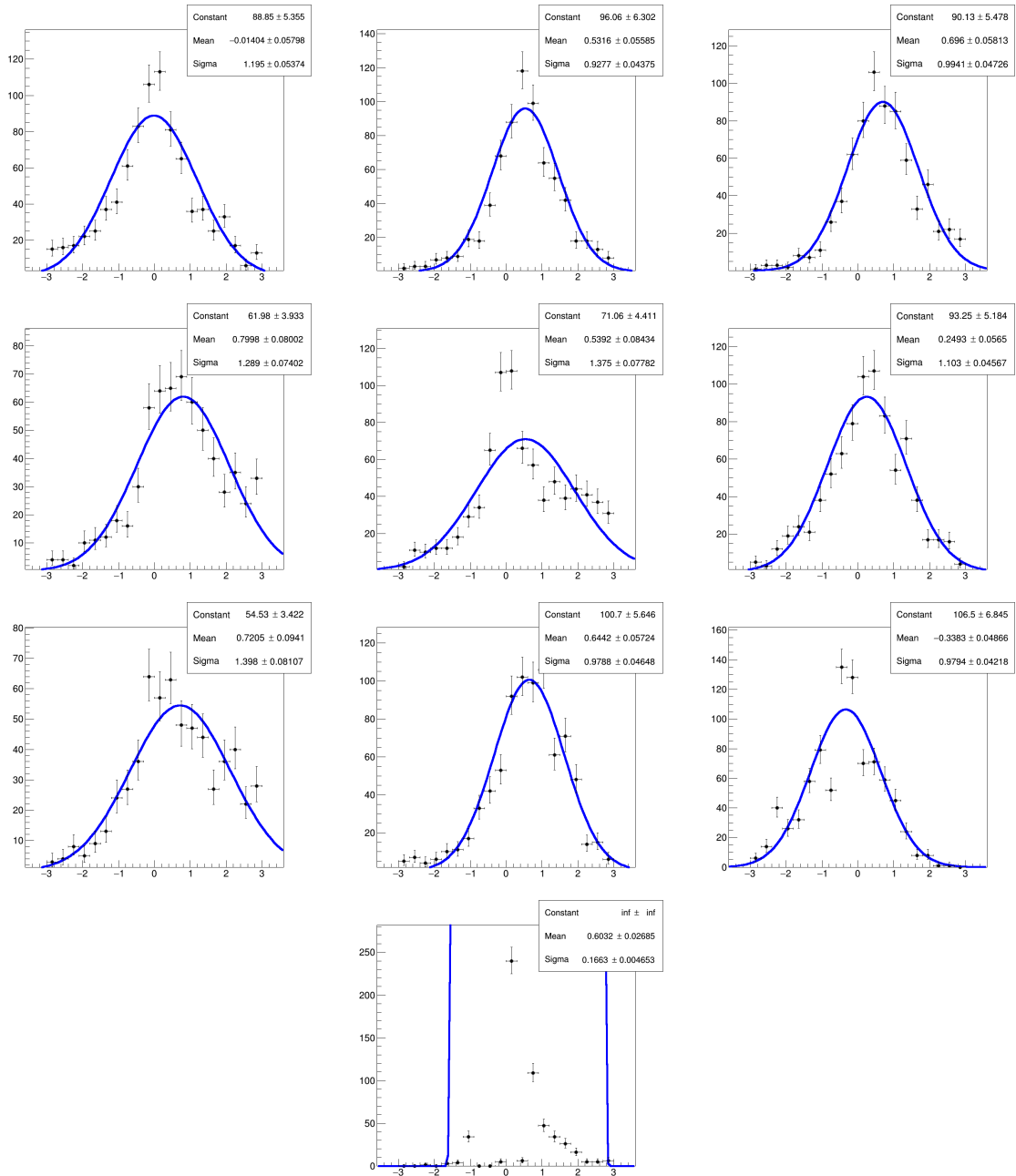


Figure 42: The closure test of FVTX South J/ψ for each FVTXN multiplicity bin is shown above. We can see overall unity pull for most of the pull distributions.

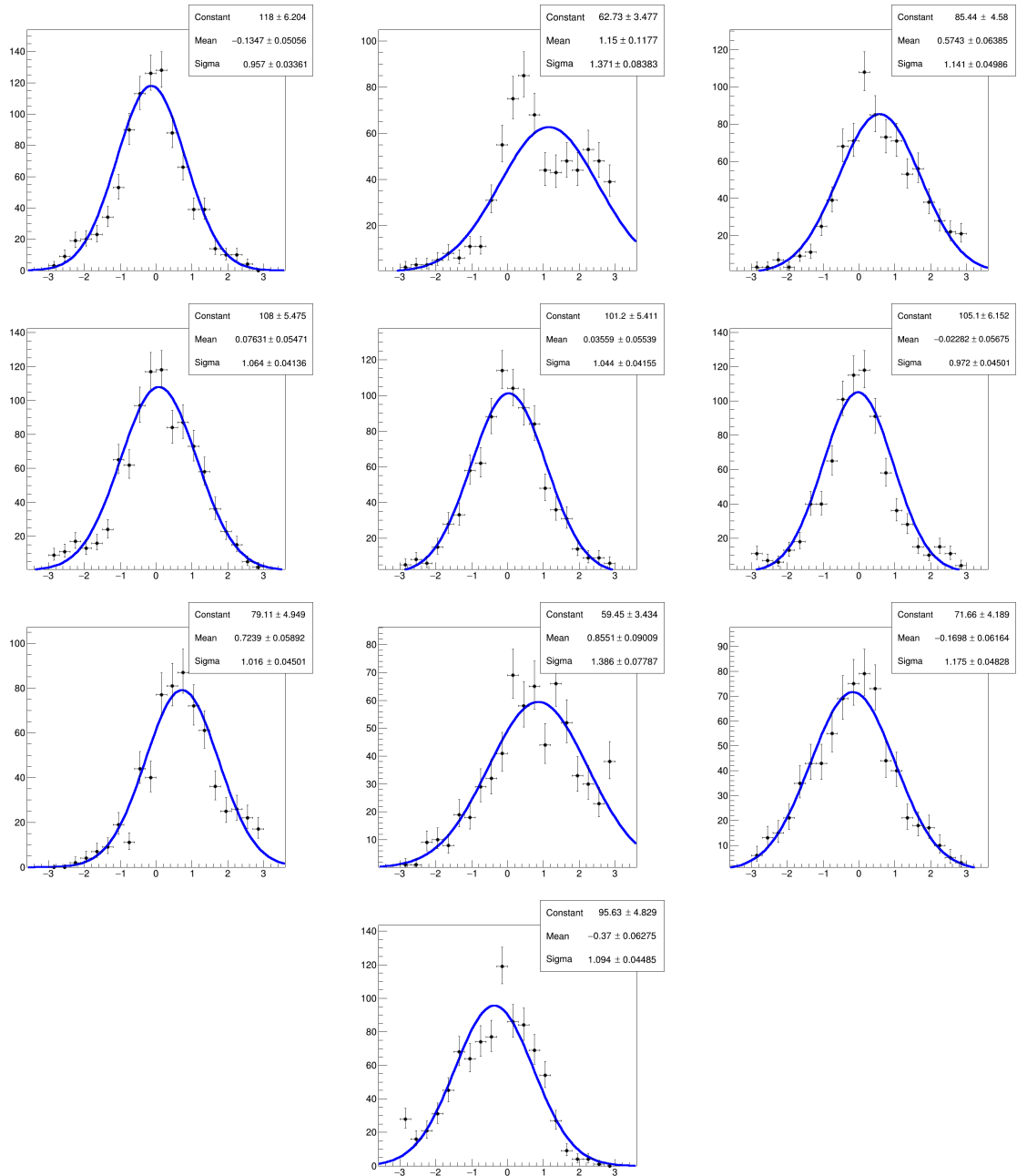


Figure 43: The closure test of FVTX South J/ψ for each FVTXS multiplicity bin is shown above. We can see overall unity pull for most of the pull distributions.

We could see that all of them are approximately unit pulls, which validate our unbinned fits.

5 Systematic Error Analysis

In this measurement, most of the detector related efficiency and acceptance variations are canceled out in the ratio.

Here we discuss a few major factors that contribute to the systematic errors in the measurements.

5.1 Event multiplicity dependent J/ψ reconstruction efficiency

The $J/\psi \rightarrow \mu^+\mu^-$ trigger and reconstruction efficiency could be affected by the global event multiplicity. In run15pp $J/\psi \rightarrow \mu^+\mu^-$ analysis (PHENIX analysis note 1354 [1]), it was found that the ...

Also in Haiwang's run13pp multiplicity analysis, it was found the J/ψ offline reconstruction efficiency is not sensitive to the E_{vtFVtx} multiplicity, see Figure 5.1. To be conservative, we assign 5% relative error to the measured J/ψ yield due to this uncertainty.

5.2 J/ψ fitting

There are systematic uncertainties from the unbinned fit in J/ψ signal raw yield extraction. To estimate the uncertainties, we vary both the signal and background function, compute the percent deviation from the nominal results, and add them into quadrature to quote them as systematic uncertainties on the fits.

Here, we vary the signal from a double Crystal Ball to a single Crystal Ball and the background from an exponential function to a linear function. Fig. 46 shows the comparison of J/ψ signal raw yields of the single Crystal Ball function as signal and linear background to the nominal fit functions:

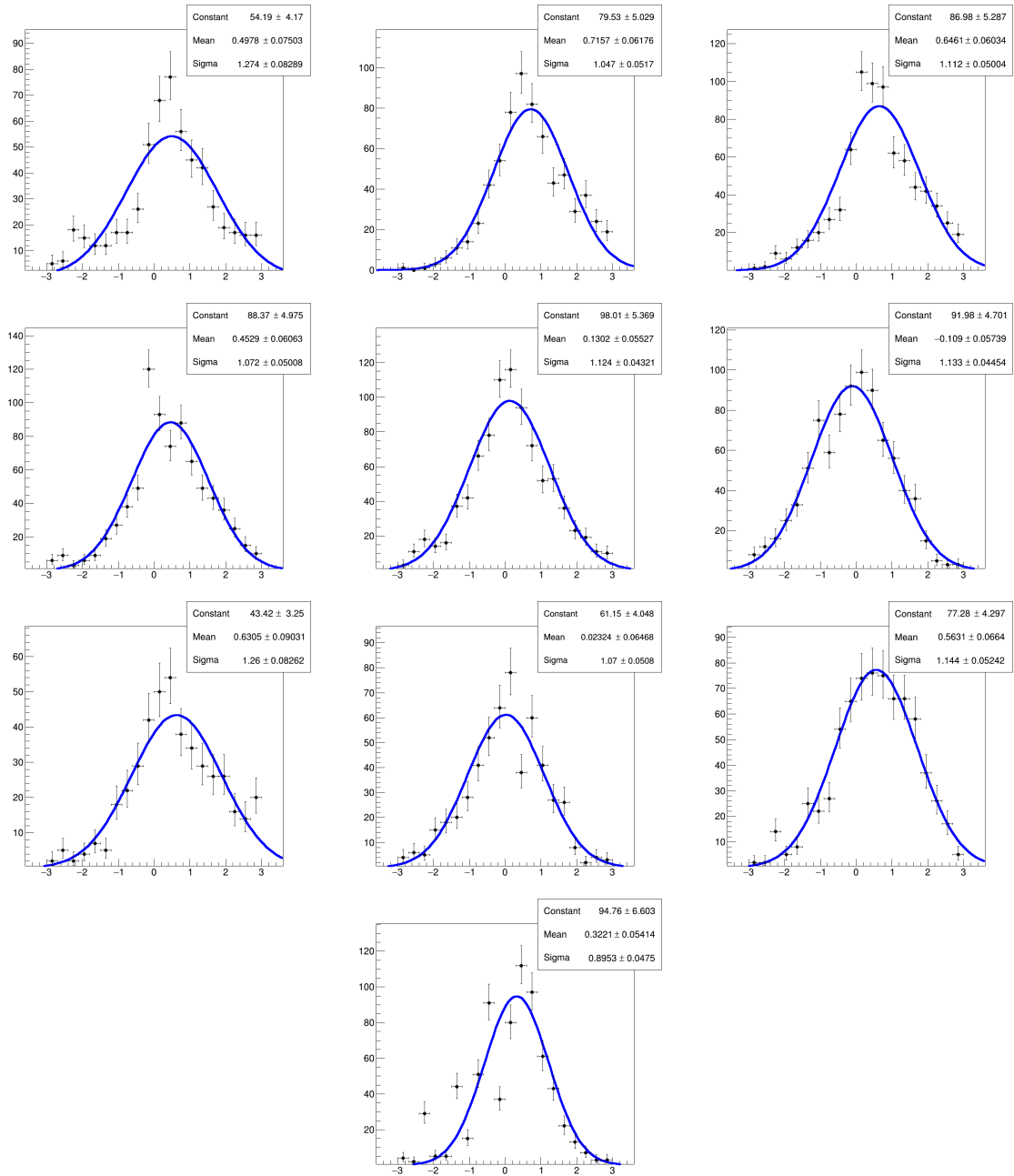


Figure 44: The closure test of FVTX South J/ψ for each FVTXS multiplicity bin is shown above. We can see overall unity pull for most of the pull distributions.

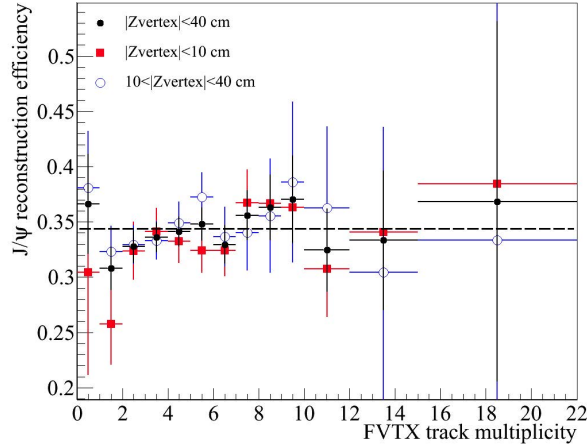


Figure 45: J/ψ reconstruction efficiency vs event multiplicity, simulation results from Haiwang's run13pp analysis (PHENIX AN1180, P17), showing 2 % uncertainty in the average reconstruction efficiency.

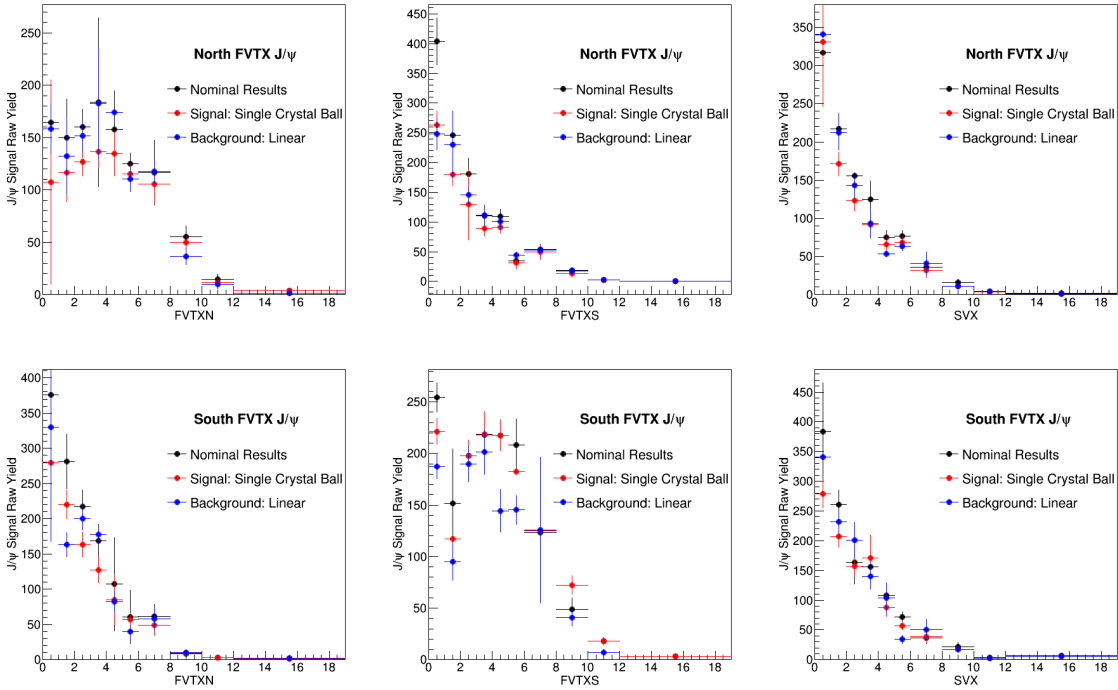


Figure 46: The FVTX North and South J/ψ signal raw yield comparisons of a single Crystal Ball function as the signal model (red) and linear function as the background model (blue) to the nominal double Crystal Ball function and exponential background (black) for each FVTXN, FVTXS, and SVX multiplicity bin are shown respectively above.

47 The percent deviation of signal and background fit variation from nominal is shown below in Figure

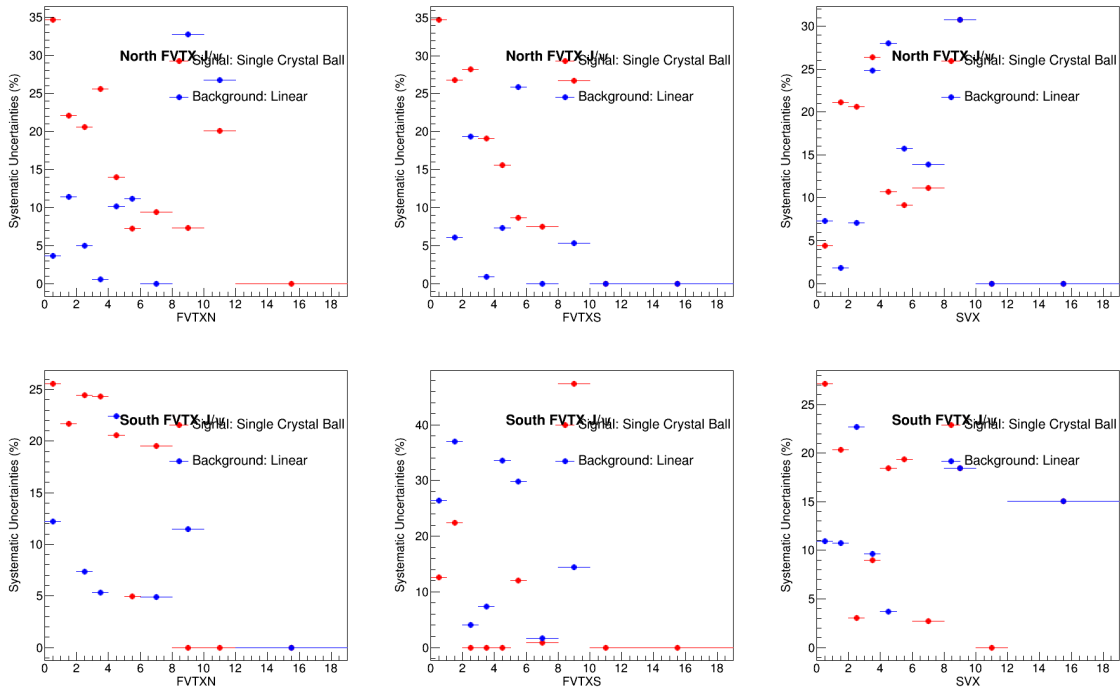


Figure 47: The FVTX North and South J/ψ signal raw yield percent deviation of using a single Crystal Ball function as the signal model (red) and a linear function as the background model (blue) for each FVTXN, FVTXS, and SVX multiplicity bin are shown respectively above.

Finally, we add the signal (σ_{sig}) and background deviations (σ_{bkg}) into quadrature and obtain the systematic uncertainties σ_{total} :

$$\sigma_{total} = \sigma_{sig} \oplus \sigma_{bkg} = \sqrt{\sigma_{sig}^2 + \sigma_{bkg}^2} \quad (14)$$

The results are shown below in Figure 48

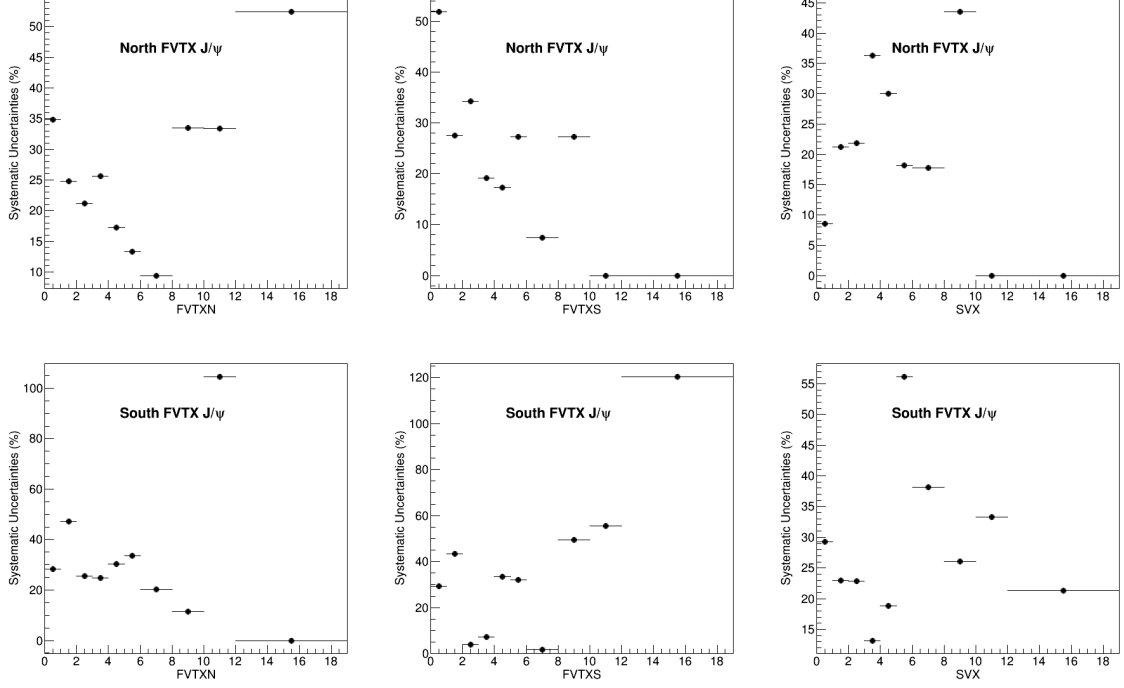


Figure 48: The FVTX North and South J/ψ signal raw yield systematic uncertainties for each FVTXN, FVTXS, and SVX multiplicity bin are shown respectively above.

Table 8 summarizes the systematic uncertainties due to the signal extraction according to our variation of signal and background:

For preliminary results, we quote a systematic uncertainty of **20%** for all the bins in the signal extraction.

5.3 MB Trigger Bias Systematic Uncertainties

We also perform studies on MB trigger bias systematic uncertainties by investigating the up/down variations of 3 different BBC rates: 600 - 800 kHz, 1000 - 1500 kHz, and 2000 - 2500 kHz. Fig. 50 shows the MB trigger bias as a function of FVTXN, FVTXS, and SVX as well as the fits to the functions at the 3 BBC rates mentioned above respectively.

Table 8: Summary of systematic uncertainties for FVTX North and South as a function of FVTXN, FVTXS, and SVX.

Event Multiplicity	N-FVTXN	N-FVTXS	N-SV	S-FVTXN	S-FVTXS	S-SV
0 - 1	34.8%	51.8%	8.5%	28.3%	29.2%	29.2%
1 - 2	24.8%	27.5%	21.2%	47.2%	43.3%	23%
2 - 3	21.2%	34.3%	21.8%	25.5%	4.04%	22.9%
3 - 4	25.6%	19.1%	36.3%	24.9%	7.34%	13.2%
4 - 5	17.2%	17.3%	30%	30.4%	33.6%	18.8%
5 - 6	13.3%	27.3%	18.2%	33.5%	32.1%	56.1%
6 - 8	9.43%	7.48%	17.8%	20.2%	1.81%	38.1%
8 - 10	33.5%	27.2%	43.5%	11.4%	49.5%	26%
10 - 12	33.4%	0%	0%	104%	55.6%	33.3%
12 - 19	52.4%	0%	0%	0%	120%	21.3%

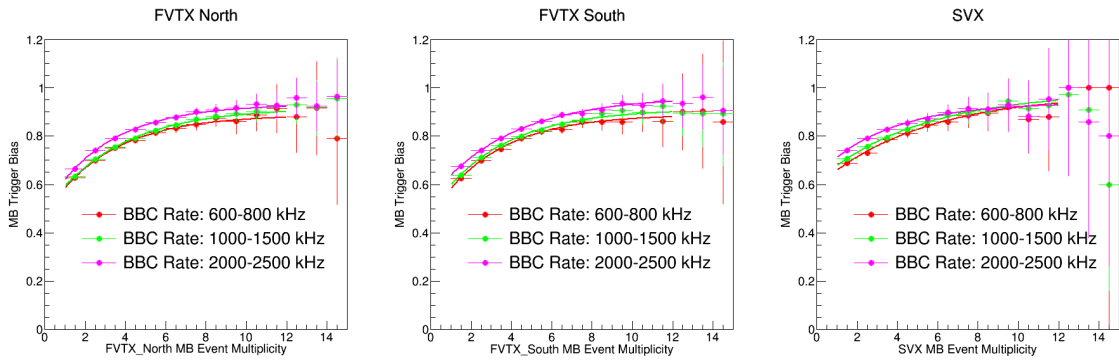


Figure 49: The MB trigger bias at BBC rate of 600 - 800 kHz (red), 1000 - 1500 kHz (green), and 2000 - 2500 kHz (magenta) for FVTXN (left), FVTXS (middle), and SVX (right) are shown above.

Then, we evaluate the bin center from the fit functions and perform the percent deviation of the high (2000 - 2500 kHz) and low (600 - 800 kHz) rates from the center (1000 - 1500 kHz) of the BBC rate. Fig. ?? shows the upper bound and lower bound of MB trigger bias systematic uncertainties for FVTXN, FVTXS, and SVX

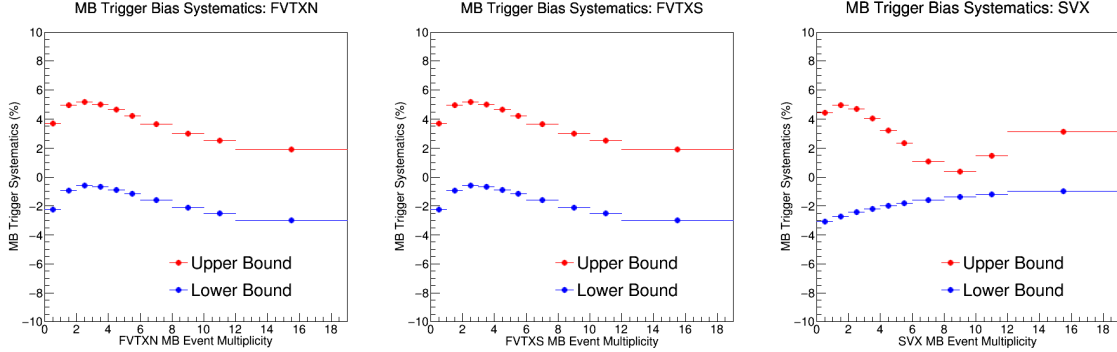


Figure 50: The upper bound (red) and lower bound (blue) of MB trigger bias systematic uncertainties for FVTXN, FVTXS, and SVX. Note that the lower bound is negative here.

Again, for preliminary results, we quote a systematic uncertainties of $\pm 5\%$ for the MB trigger bias systematic uncertainties, as discussed in previous section.

5.4 Systematic Uncertainties on the Evaluation of Multiple Collisions

For preliminary results, we quote a systematic uncertainty of 20% for the correction of evaluation of multiple collisions. We plan to explore run by run correction (or group runs according to BBC rate) to reduce this uncertainty.

5.5 Systematic Uncertainties on J/ψ Reconstruction

For preliminary results, we quote a systematic uncertainty of 15% for the correction of J/ψ reconstruction as discussed in previous section.

5.6 Summary of Systematic Uncertainties

Finally, based on our studies of different sources of systematic uncertainties above, we put together all the systematic uncertainties for each bin for North and South FVTX J/ψ as functions of FVTXN, FVTXS, and SVX.

Currently, we quote a uniform systematic uncertainty for each bin by adding all sources of systematic uncertainties in quadrature:

$$\sigma_{TotalSyst} = \sigma_{Fit} \oplus \sigma_{TrigBias} \oplus \sigma_{MultColl} \oplus \sigma_{J/\psi Reco} \quad (15)$$

$$\sigma_{TotalSyst} = \sqrt{20\%^2 + 5\%^2 + 20\%^2 + 15\%^2} = 32.4\% \quad (16)$$

Table 9 summarizes all sources of systematic uncertainties and compute the total systematic uncertainties for each multiplicity bin:

Table 9: Summary of the total of all sources of systematic uncertainties each multiplicity bin.

Event Multiplicity	N-FVTXN	N-FVTXS	N-SV	S-FVTXN	S-FVTXS	S-SV
0 - 1	32.4%	32.4%	32.4%	32.4%	32.4%	32.4%
1 - 2	32.4%	32.4%	32.4%	32.4%	32.4%	32.4%
2 - 3	32.4%	32.4%	32.4%	32.4%	32.4%	32.4%
3 - 4	32.4%	32.4%	32.4%	32.4%	32.4%	32.4%
4 - 5	32.4%	32.4%	32.4%	32.4%	32.4%	32.4%
5 - 6	32.4%	32.4%	32.4%	32.4%	32.4%	32.4%
6 - 8	32.4%	32.4%	32.4%	32.4%	32.4%	32.4%
8 - 10	32.4%	32.4%	32.4%	32.4%	32.4%	32.4%
10 - 12	32.4%	32.4%	32.4%	32.4%	32.4%	32.4%
12 - 19	32.4%	32.4%	32.4%	32.4%	32.4%	32.4%

6 Results

6.1 \hat{Y} vs \hat{N}_{trk} Before Corrections

Now, with all the ingredient including the J/ψ signal raw yield $N^{J/\psi}$ to evaluate the normalized yield \hat{Y} as a function of FVTXN, FVTXS, and SVX N_{trk} multiplicity.

The $\langle\sigma^{J/\psi}\rangle/\langle\sigma^{\text{MB}}\rangle = \langle N^{J/\psi}\rangle/\langle N^{\text{MB}}\rangle$.

$\langle N^{J/\psi}\rangle$ is the average number of J/ψ defined as: ratio of total number of J/ψ to the total number of events.

$\langle N^{\text{MB}}\rangle$ is the average multiplicity of MB events, which has a value about 1.5.

We further scale the x-axis $\hat{N}_{\text{trk}} = N_{\text{trk}}/\langle N_{\text{trk}}\rangle$. Putting all these together, we get the \hat{Y} for FVTX North and South muon as a function of FVTXN, FVTXS, and SVX tracklet multiplicity N_{trk} , shown in Fig. 51 and Fig. 52 respectively.

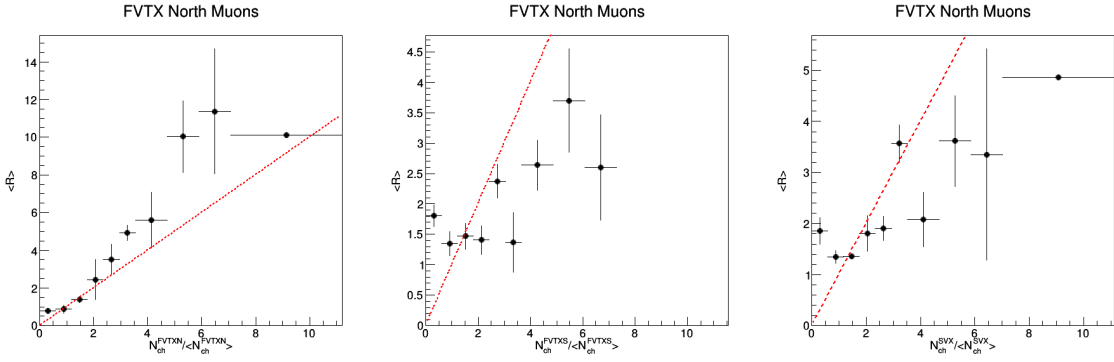


Figure 51: The normalized FVTX North J/ψ yield \hat{Y} as a function FVTX North (left), FVTX South (middle), and SVX (right) tracklet multiplicity in PHENIX Run 15 $p + p$ collisions are shown above.

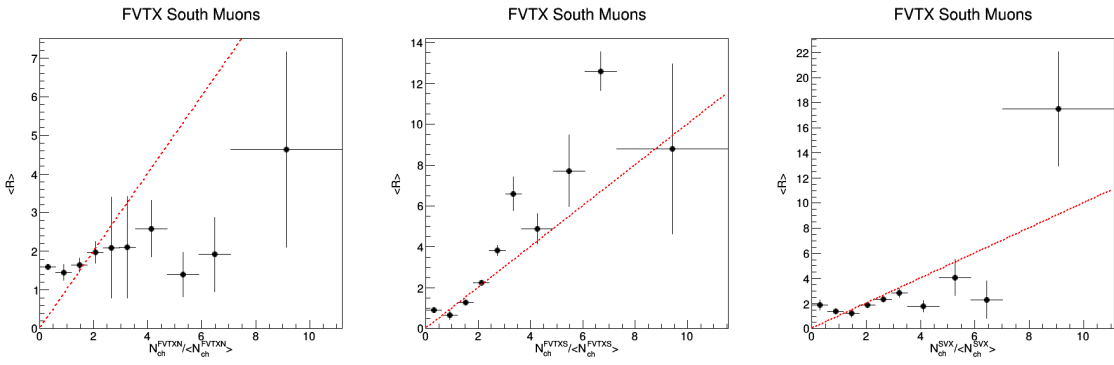


Figure 52: The normalized FVTX South J/ψ yield \hat{Y} as a function FVTX North (left), FVTX South (middle), and SVX (right) tracklet multiplicity in PHENIX Run 15 $p + p$ collisions are shown above.

6.2 \hat{Y} vs \hat{N}_{trk} After Corrections

Finally, we could put in the corrections of MB trigger bias and multiple collection factors by evaluate the bin center of our fit functions. In addition, we could perform a linear fit: $y = mx + n$ to the normalized yields to obtain the slope, x-intercept, and y-intercept.

Figure 53 and Figure 54 respectively show the trigger bias and multiple collision corrected normalized yield \hat{Y} of FVTX North and South J/ψ as a function of normalized FVTXN, FVTXS, and SVX

tracklet multiplicity \hat{N}_{trk} . In addition, we compare them to the reference line: $y = x$ (red) and the linear fits (green).

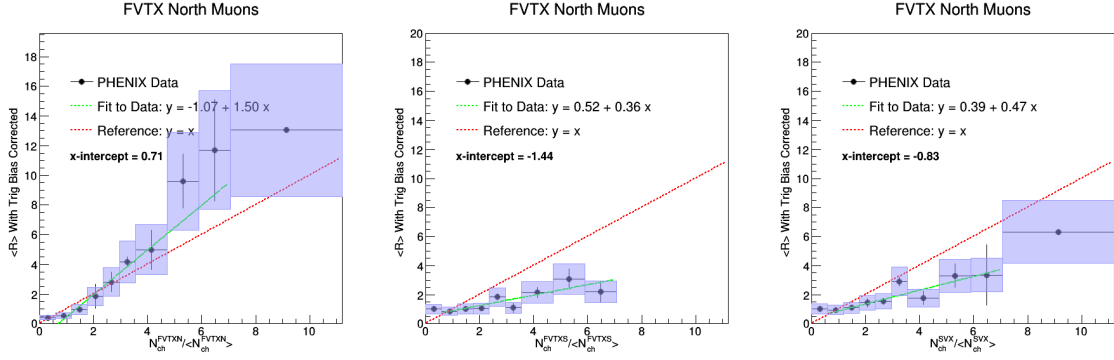


Figure 53: The trigger bias and multiple collision corrected normalized FVTX North J/ψ yield \hat{Y} as a function FVTX North (left), FVTX South (middle), and SVX (right) tracklet multiplicity in PHENIX Run 15 pp collisions are shown above. We also compare it with the reference line $y = x$ (red) and the linear fit $y = mx + n$. The blue box represents the systematic uncertainty for each data point.

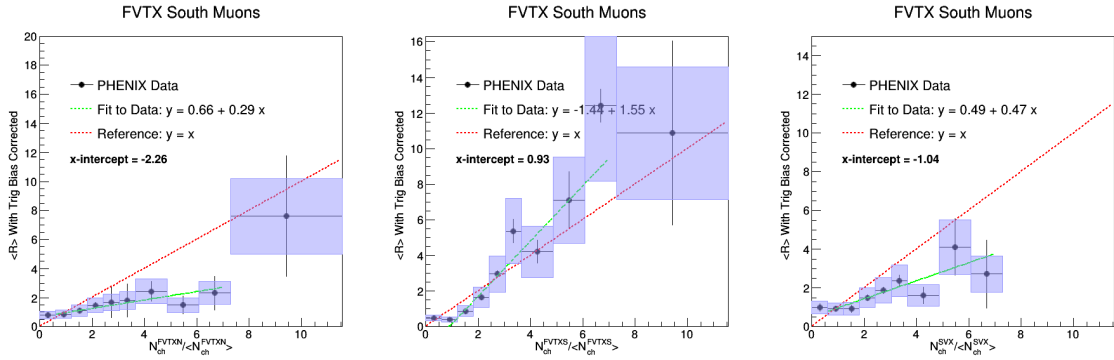


Figure 54: The trigger bias and multiple collision corrected normalized FVTX South J/ψ yield \hat{Y} as a function FVTX North (left), FVTX South (middle), and SVX (right) tracklet multiplicity in PHENIX Run 15 pp collisions are shown above. We also compare it with the reference line $y = x$ (red) and the linear fit $y = mx + n$. The blue box represent the systematic uncertainty for each data point

According to our linear fit results, we could see that in the same arm (ie. FVTXN N_{trk} for North J/ψ and FVTXS N_{trk} for South J/ψ), the slopes are greater than 1 while the x- and y-intercepts are more negative than the opposite arm (ie. FVTXS N_{trk} for North J/ψ and FVTXN N_{trk} for South J/ψ) where the slopes are less than 1 while the x- and y-intercept are closer to 0. For SVX, the slopes are less than 1 but the x- and y- intercepts are close to 0.

Finally, we plot the North and South FVTX J/ψ together along with the reference line $y = x$ and the linear fit functions for FVTXN, FVTXS, and SVX as shown in Figure 55 below:

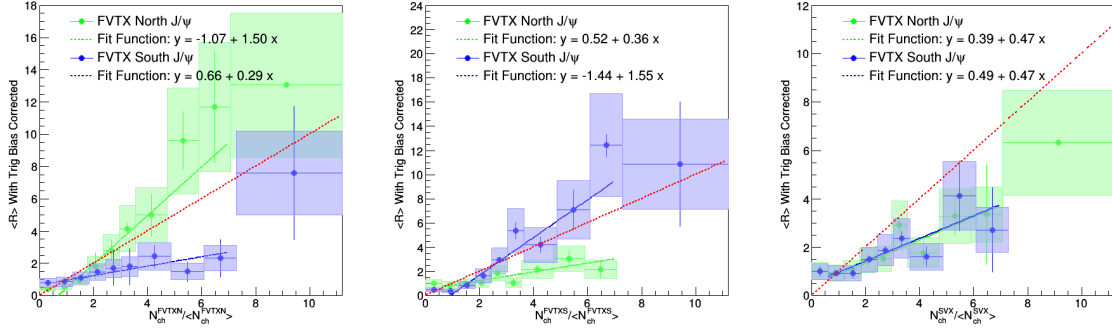


Figure 55: The trigger bias and multiple collision corrected normalized FVTX South J/ψ yield \hat{Y} as a function FVTX North (left), FVTX South (middle), and SVX (right) tracklet multiplicity in PHENIX Run 15 pp collisions are shown above. We also compare it with the reference line $y = x$ (red) and the linear fit $y = mx + n$. The blue and green boxes represent the systematic uncertainty for FVTX North and South J/ψ data points respectively

Finally, the fit parameters: the slope m , the y-intercept: n , and the x-intercept $-n/m$ are summarized below in Table 10

Table 10: Summary of the total of all sources of systematic uncertainties each multiplicity bin.

Event Multiplicity Plots	Slope m	y-intercept n	x-intercept $-n/m$
North FVTX J/ψ for FVTXN	-1.07 ± 0.20	1.50 ± 0.13	0.71 ± 0.15
North FVTX J/ψ for FVTXS	0.52 ± 0.15	0.358 ± 0.070	-1.44 ± 0.50
North FVTX J/ψ for SVX	0.39 ± 0.11	0.474 ± 0.073	-0.83 ± 0.26
South FVTX J/ψ for FVTXN	0.66 ± 0.16	0.290 ± 0.092	-2.26 ± 0.90
South FVTX J/ψ for FVTXS	-1.44 ± 0.15	1.552 ± 0.084	0.93 ± 0.11
South FVTX J/ψ for SVX	0.49 ± 0.13	0.467 ± 0.067	-1.04 ± 0.31

References

- [1] Matt Durham, Sanghoon Lim, and Pat McGaughey. Ratios of $\psi(2s)/\psi(1s)$ from runs 14 and 15 with the fvtx. *PHENIX Analysis Note 1240*, 2019.
- [2] J. Gaiser. [Charmonium Spectroscopy From Radiative Decays of the \$J/\psi\$ and \$\psi'\$](#) , Ph.D. Thesis, SLAC, 1982.
- [3] Haiwang Yu, Cesar da Silva, Jin Huang, Ming Liu, Xiaorong Wang, and Melynda Brooks. Phenix run13 jpsi analysis. *PHENIX Analysis Note 1180*, 2014.